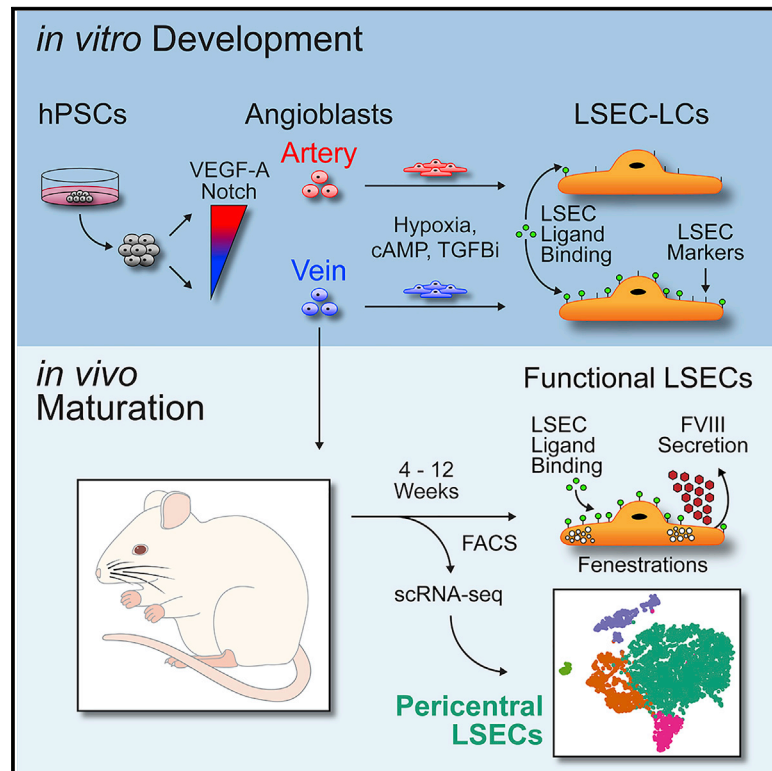


Generation of Functional Liver Sinusoidal Endothelial Cells from Human Pluripotent Stem-Cell-Derived Venous Angioblasts

Graphical Abstract



Authors

Blair K. Gage, Jeff C. Liu,
Brendan T. Innes,
Sonya A. MacParland,
Ian D. McGilvray, Gary D. Bader,
Gordon M. Keller

Correspondence

blair.gage@uhnresearch.ca (B.K.G.),
gordon.keller@uhnresearch.ca (G.M.K.)

In Brief

Gage et al. show that hPSC-derived venous endothelial cells are better able to upregulate markers of LSECs *in vitro* and *in vivo* compared to arterial cells. Upon intrahepatic neonatal and adult transplantation, venous progenitors engrafted, proliferated, and matured into recoverable functional hPSC-derived LSECs with characteristics similar to primary human LSECs.

Highlights

- VEGF-A and Notch signaling regulate arteriovenous specification in hPSCs
- Venous endothelial cells upregulate LSEC markers more robustly than arterial cells
- Venous angioblasts humanize neonatal and adult NSG mouse liver sinusoids
- hPSC-LSECs are functionally mature (fenestrated, scavenging, and produce FVIII)

Article

Generation of Functional Liver Sinusoidal Endothelial Cells from Human Pluripotent Stem-Cell-Derived Venous Angioblasts

Blair K. Gage,^{1,*} Jeff C. Liu,² Brendan T. Innes,^{2,6} Sonya A. MacParland,^{3,4,5} Ian D. McGilvray,³ Gary D. Bader,^{2,6} and Gordon M. Keller^{1,7,8,*}

¹McEwen Stem Cell Institute, University Health Network, Toronto, ON M5G1L7, Canada

²The Donnelly Center, University of Toronto, Toronto, ON M5S3E1, Canada

³Multi-Organ Transplant Program, Toronto General Hospital Research Institute, Toronto, ON M5G2C4, Canada

⁴Department of Immunology, University of Toronto, Toronto, ON, M5S1A8, Canada

⁵Department of Laboratory Medicine and Pathobiology, University of Toronto, Toronto, ON M5G1L7, Canada

⁶Department of Molecular Genetics, University of Toronto, Toronto, ON M5G1A8, Canada

⁷Department of Medical Biophysics, University of Toronto, Toronto, ON M5G1L7, Canada

⁸Lead Contact

*Correspondence: blair.gage@uhnresearch.ca (B.K.G.), gordon.keller@uhnresearch.ca (G.M.K.)

<https://doi.org/10.1016/j.stem.2020.06.007>

SUMMARY

Liver sinusoidal endothelial cells (LSECs) form a highly specialized microvasculature that plays a critical role in liver function and disease. To better understand this role, we developed a strategy to generate LSECs from human pluripotent stem cells (hPSCs) by first optimizing the specification of arterial and venous angioblasts and derivative endothelial populations. Induction of a LSEC-like fate by hypoxia, cyclic AMP (cAMP) agonism, and transforming growth factor β (TGF- β) inhibition revealed that venous endothelial cells responded more rapidly and robustly than the arterial cells to upregulate LSEC markers and functions *in vitro*. Upon intrahepatic transplantation in neonates, venous angioblasts engrafted the liver and generated mature, fenestrated LSECs with scavenger functions and molecular profiles of primary human LSECs. When transplanted into the liver of adult mice, angioblasts efficiently gave rise to mature LSECs with robust factor VIII (FVIII) production. Humanization of the murine liver with hPSC-derived LSECs provides a tractable system for studying the biology of this key liver cell type.

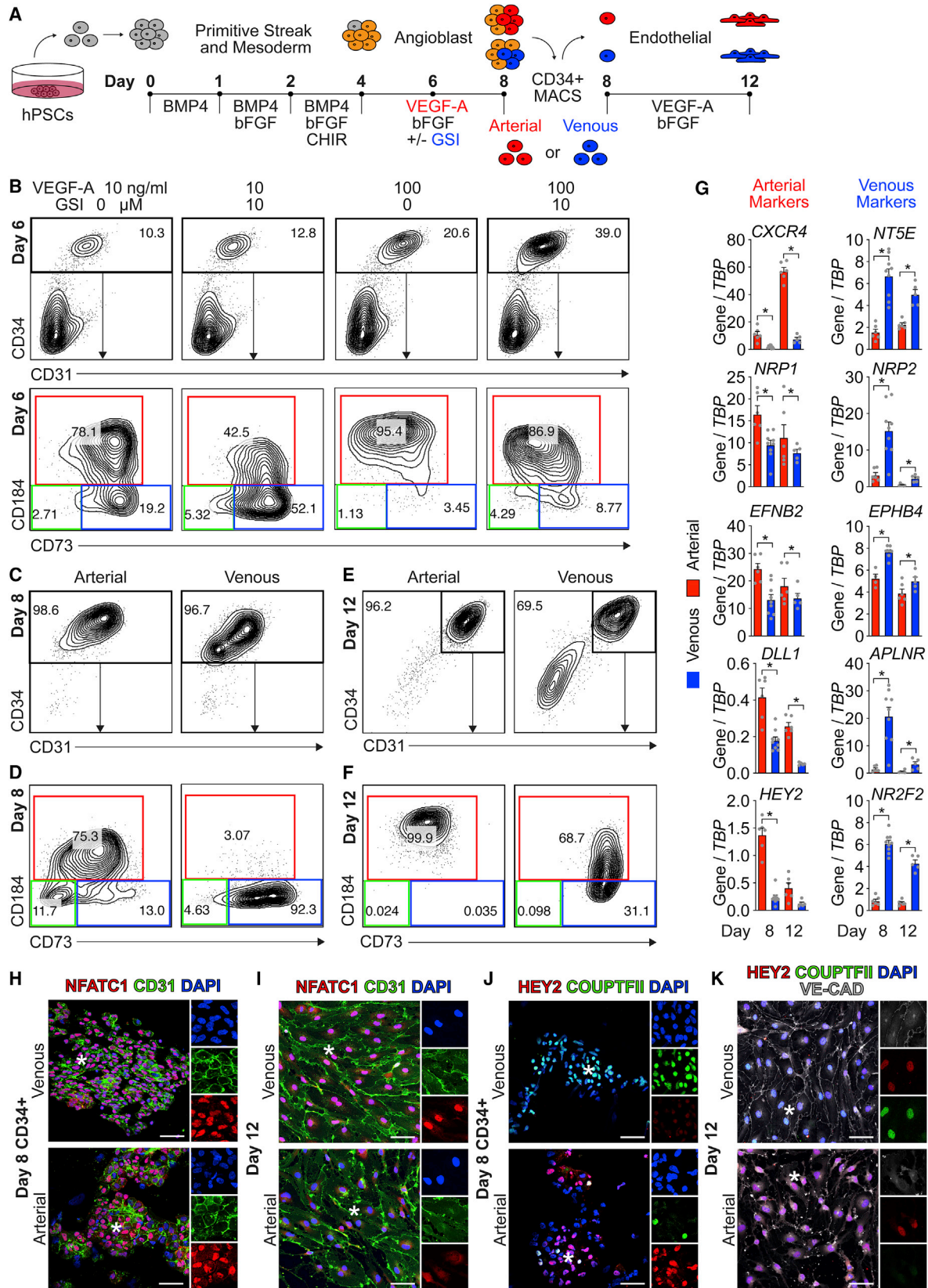
INTRODUCTION

The vasculature of the liver is an anatomically specialized structure where oxygenated arterial and nutrient-rich portal venous blood mix within a sinusoidal space that drains into a hypoxic central vein. The sinusoids are lined with unique endothelial cells known as liver sinusoidal endothelial cells (LSECs) that are distinguished from other endothelial cells by their reduced levels of expression of CD34, CD31 (*PECAM1*), and von Willebrand factor (VWF) and elevated expression of LYVE1, CD14, CD32B (*FCGR2B*), CD36, CD54, STAB1, STAB2, CLEC1B, and factor VIII (FVIII) (*F8*) (Fomin et al., 2013, 2017; Halpern et al., 2018; MacParland et al., 2018; Shahani et al., 2014; Strauss et al., 2017) and the presence of transcellular fenestrations arranged in sieve plates (Wisse et al., 1985). These distinct characteristics allow LSECs to carry out a number of critical functions within the liver, including the transport of metabolic blood components and drugs to hepatocytes through fenestrations, scavenging, and clearing of biomolecules from the blood and the secretion of the coagulation factor FVIII (Braet and Wisse, 2002; Deleve, 2013a; Elvevold et al., 2008b; Wisse et al., 1985). Additionally,

LSECs have been shown to play an important role in hepatic regeneration following liver injury (Ding et al., 2010, 2014; Hu et al., 2014).

Given their central role in normal liver homeostasis, loss of LSEC function is associated with a number of human diseases. These include hemophilia A, caused by a deficiency in LSEC-derived FVIII; sinusoidal obstruction syndrome (SOS) resulting from drug-induced toxicity to LSECs; and certain forms of chronic liver disease where LSECs defenestrate and promote fibrosis at the expense of regeneration (Deleve, 2013a). In these cases, LSECs represent a clinically relevant source of FVIII, the earliest cell lost during acute drug-related liver damage, and a central regulator of hepatic regeneration/fibrosis. As such, LSECs, or LSEC progenitors, represent a promising cell population for studying the events that lead to liver disease and organ failure and developing new cellular therapies to treat these conditions.

Detailed studies on the role of LSECs in liver function and disease and the development of potential new LSEC-based therapies is dependent on our ability to access these cells. As access to primary human LSECs from cadaveric livers is limited by



(legend on next page)

ischemic sensitivity and organ availability, human pluripotent stem cells (hPSCs) are now being considered as an alternative source of these cells. As with most cell types, the successful derivation of functional LSECs from hPSCs will depend on our ability to translate the key aspects of their development in the embryo to the differentiation cultures. Lineage-tracing studies in the mouse provide evidence that the vasculature of the liver, including LSECs, is of venous origin and derived from NFATC1⁺ NPR3⁻ sinus venosus progenitors and the early hepatic portal circulatory system (Hen et al., 2015; Zhang et al., 2016). Venous and arterial fates are established early during embryogenesis as the angioblasts are specified from lateral plate mesoderm through the coordinated interaction of different signaling pathways, including hedgehog, vascular endothelial growth factor (VEGF), and Notch (Fish and Wythe, 2015; Zhong et al., 2001). Although the regulators of LSEC specification are not well understood, studies have shown that the adrenomedullin/RAMP2 pathway plays a role in this process, as disruption of signaling within the endothelial lineage leads to liver cirrhosis and immune cell infiltration associated with LSEC detachment from the sinusoidal walls (Ichikawa-Shindo et al., 2008; Koyama et al., 2013; Shindo et al., 2001). As the liver matures, LSECs populate three diverse hepatic metabolic zones (zones 1–3) that provide additional regional specific cues, including gradients in oxygen, nutrients, hormones, cytokines, and extracellular matrices to further direct their maturation (Ben-Moshe and Itzkovitz, 2019; Halpern et al., 2017, 2018).

Several studies have reported on the derivation of LSEC-like cells from both mouse pluripotent stem cells (mPSCs) and hPSCs. Using the mouse embryonic stem cell (ESC) model, Arai et al. (2011) showed that the combination of adrenomedullin and transforming growth factor β (TGF- β) inhibition led to increased expression of LSEC related genes in embryoid body (EB) outgrowth endothelial cells. Building on their previous mouse ESC work (Nonaka et al., 2008), Kouï et al. demonstrated that inhibition of TGF- β signaling in human induced pluripotent stem cell (hiPSC)-derived KDR⁺CD34⁺CD31⁺ vascular cells promoted the development of a CD32⁺ subpopulation that expressed *STAB2* and *F8* at levels comparable to *in vitro*-expanded, commercially available human hepatic endothelial cells (Kouï et al., 2017). While these studies indicate that it is possible to generate LSEC-like cells from PSCs, the arterial or venous origin of the cells was not assessed prior to specification. Additionally, the levels of maturation of the populations were not fully characterized as comparisons were not made to primary LSECs.

To gain a better understanding of development of the LSEC lineage from hPSCs, we focused our efforts on first generating

properly specified venous angioblasts through manipulation of the VEGF-A and Notch pathways and then subjecting these progenitors to appropriate signaling cues *in vitro* and *in vivo*. We show that venous progenitors responded more rapidly and robustly than arterial cells to upregulate markers of the LSEC lineage in response to cyclic AMP (cAMP), TGF- β inhibition, and hypoxia. Transplantation studies revealed that venous angioblasts are best able to engraft, expand, and differentiate into cells that display the hallmarks of adult LSECs, including marker expression, fenestration, ligand scavenging, and FVIII secretion. Taken together, these studies emphasize the critical roles of both developmental and anatomical signaling mechanisms in regulating the generation of sinusoidal endothelial cells from hPSCs.

RESULTS

Specification of Artery and Venous Angioblasts from hPSCs

For these studies, hPSCs were differentiated using our previously described EB-based protocol that involves the sequential addition of bone morphogenetic protein 4 (BMP4; days 0–4), basic fibroblast growth factor (bFGF; days 1–8) and CHIR (days 2–4) for the induction of KDR⁺CD56⁺CD235a/b⁻ mesoderm at day 4 of differentiation (Figures 1A and S1A) (Sturgeon et al., 2014). Addition of VEGF (VEGF-A) on day 4 induced the development of angioblasts by days 6–8 that expressed markers indicative of early vascular development including CD34, CD31, CD184/*CXCR4* and CD73/*NT5E* (Figure S1B) (Ditadi et al., 2015).

To generate venous angioblasts as a potential source of LSECs (Hen et al., 2015; Zhang et al., 2016), we next examined the role of VEGF-A, bFGF, and Notch signaling as these pathways have been shown to regulate early arteriovenous specification during hPSC differentiation (Ditadi et al., 2015; Zhang et al., 2017). To optimize venous and arterial development in our cultures, we manipulated VEGF-A and basic fibroblast growth factor (bFGF) concentrations between days 4 and 6 of differentiation. At day 6, the populations were analyzed for the presence of CD34⁺CD31^{low} early angioblasts that displayed arterial (CD34⁺CD184⁺CD73^{low}) or venous (CD34⁺CD184⁻CD73⁺) fates (Ditadi et al., 2015). Increasing VEGF-A concentrations up to 100 ng/mL led to significant, dose-dependent increases in CD34⁺ angioblast frequency at all concentrations of bFGF tested (Figures 1B and S1C). High concentrations of VEGF-A (30 and 100 ng/mL) promoted the development of a CD34⁺CD184⁺CD73^{low} arterial-like population, whereas low/no VEGF-A (0 and 10 ng/mL) generated a CD34⁺CD184⁻CD73⁺ venous-like

Figure 1. Generation of Arterial and Venous Angioblasts and Derivative Endothelial Cells

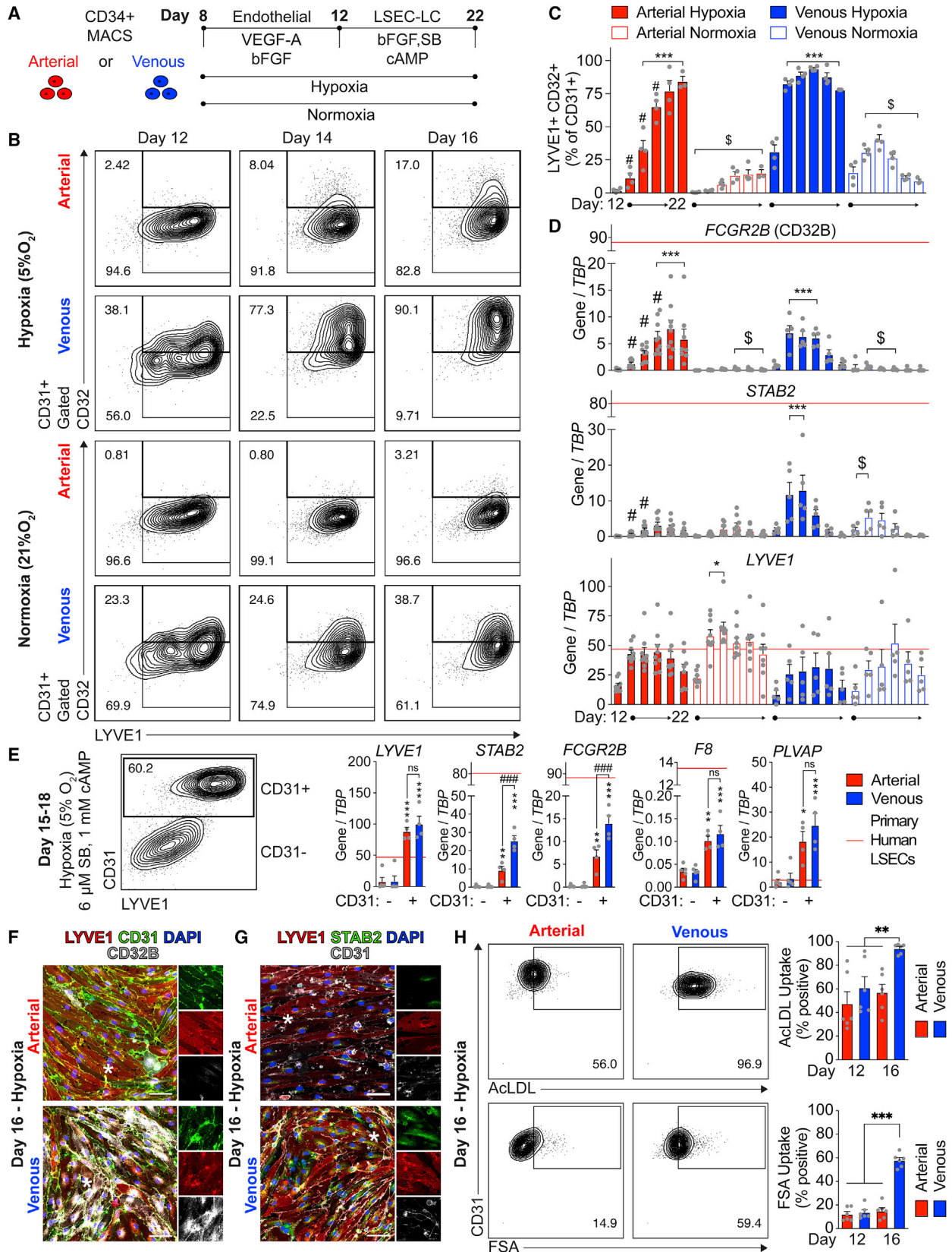
(A) Schematic of arterial and venous differentiation to angioblasts and endothelial cells.

(B) Flow cytometric analysis of day 6 CD34⁺ angioblasts specified under indicated day 4–6 treatment conditions of VEGF-A (10 or 100 ng/mL), bFGF (30 ng/mL), and GSI (0 or 10 μ M). See Figures S1B and S1C for quantification.

(C–F) Flow cytometric analysis of MACS-isolated day 8 arterial (day 4–8: 100 ng/mL VEGF-A and 30 ng/mL bFGF) and venous (day 4–8: 10 ng/mL VEGF-A, 30 ng/mL bFGF, and 10 μ M GSI) angioblasts (C and D) and derivative endothelial cells grown for 4 days (E and F). Patterns in (D) and (F) are from the gated CD34⁺ fractions in (C) and (E).

(G) qRT-PCR analysis of arterial and venous markers in day 8 CD34⁺ angioblasts and day 12 CD31⁺ endothelial cells. Values are normalized to *TBP* (mean \pm SEM, two-way ANOVA * p < 0.05 artery versus vein on given day).

(H–K) Immunofluorescence of cytospun day 8 CD34⁺ venous and arterial angioblasts and day 12 monolayer expanded endothelial cells counterstained with DAPI. (H) NFATC1 and CD31 expression in day 8 cells and (I) NFATC1 and CD31 expression in day 12 cells. (J) HEY2 and COUPTFII expression in day 8 cells and (K) HEY2, COUPTFII, and VE-CAD expression in day 12 cells. Scale bar represents 50 μ m. **** indicates location of enlarged single-channel inset panels.



(legend on next page)

population (Figures 1B and S1C). Increasing bFGF doses had little effect on arteriovenous specification but increased total cell number (Figure S1C). To investigate the role of Notch signaling, the gamma-secretase inhibitor (GSI: L-685-458) was added at different concentrations at day 4 during the arterial (100 ng/mL VEGF-A)/venous (10 ng/mL VEGF-A) specification step. Notch inhibition maintained or increased CD34 frequency and reduced the proportion of CD184⁺ cells (arterial) and increased the frequency of CD184⁻CD73⁺ (venous) cells under low, but not high, VEGF-A conditions (Figures 1B and S1D). Taken together, these data show that specification of KDR⁺ mesoderm with Notch inhibition and low concentrations of VEGF-A promote the development of a CD34⁺CD184⁻CD73⁺ venous-like population, while high concentrations of VEGF-A specify a CD34⁺CD184⁺CD73^{low} arterial-like population.

To further enrich the venous angioblast populations, we extended Notch inhibition to day 8 to reduce CD184⁺ arterial-like cell contamination. Analyses of magnetic-activated cell sorting (MACS) isolated day 8 CD34⁺ cells showed that prolonged Notch inhibition resulted in the development of populations enriched for venous-like cells (86% ± 2% CD184⁻CD73⁺) (Figures 1C, 1D, S1F, and S1G). To promote differentiation of the angioblasts to endothelial cells, day 8 CD34⁺CD31^{low} venous and arterial populations were expanded for 4 days in monolayer culture in the presence of bFGF and VEGF-A without Notch inhibition. During this culture, ~40% of the venous population lost CD34 and CD31 expression and upregulated PDGFRβ (Figure S1I). The persisting CD34⁺CD31⁺ venous endothelial cells retained high CD73 expression and upregulated CD184 (Figures 1F, S1G, and S1H), a pattern observed in migrating venous tip vascular cells *in vivo* (Hasan et al., 2017). In contrast, most arterial cells retained CD34 and upregulated CD31 and CD184 expression (>95%) (Figures 1E, 1F, S1F, and S1G). qRT-PCR expression analyses revealed that day 8 arterial angioblasts expressed higher levels of the arterial makers *CXCR4*, *NRP1*, and *EFNB2* and the Notch signaling components *DLL1* and *HEY2* than venous angioblasts (Figure 1G). Venous angioblasts expressed higher levels of the venous markers *NT5E*, *NRP2*, *EPHB4*, *APLNR*, and *NR2F2/COUPTFII*. These differential expression patterns were retained following the 4-day monolayer expansion culture. Immunocytochemical analysis showed that NFATC1 protein was detected in both populations of angioblasts but preferentially retained in the nucleus of venous cells following the 4-day culture period (Figures 1H–1K). COUPTFII was largely restricted to the

venous cells at both 8 and 12 days of culture, whereas HEY2 was found at higher levels in arterial lineage cells (Figures 1H–1K).

Taken together, these findings confirm that it is possible to generate arterial and venous vascular cells from hPSCs through the stage-specific modulation of the VEGF-A, bFGF, and Notch signaling pathways.

In Vitro Specification of LSEC-like Cells (LSEC-LCs) from Arterial and Venous Endothelial Lineages

To generate LSECs from day 12 venous cells, we treated the cultures every 2 days for 4 days with modulators of pathways implicated in LSEC specification, including 8-Br-cAMP (cAMP), a known mediator of adrenomedullin signaling; the TGF-β inhibitor SB431542 (SB); and VEGF-C (Arai et al., 2011; Ding et al., 2010; Hippenstiel et al., 2002; Kouji et al., 2017; Nonaka et al., 2008) (Figure S2A). qRT-PCR analyses showed that cAMP alone led to the upregulation of the LSEC scavenger receptors *LYVE1*, *STAB2*, and *FCGR2B*, while inhibition of TGF-β alone induced the expression of *STAB2* and *FCGR2B*, but not *LYVE1* (Figure S2B). Combining these two pathway modulators induced the highest expression levels of these genes and the coagulation factor *F8*. Although VEGF-C modestly enhanced LSEC marker expression, it also increased the expression levels of the lymphatic markers *PROX1* and *FLT4*. Given this, we used the combination of SB (6 μM) and cAMP (1 mM) to induce a LSEC-like fate for the studies described below.

Treatment of day 12 venous cells with SB and cAMP for 4 days resulted in the development of CD31⁺LYVE1⁺ and CD31⁻LYVE1⁻ subpopulations (Figure S2C). Molecular analyses revealed that the CD31⁺ cells expressed significantly higher levels of *LYVE1*, *STAB2*, *FCGR2B*, and *F8* than the CD31⁻ cells, indicating that this endothelial population contains hPSC-derived LSEC-LCs. While *LYVE1*, *STAB2*, and *FCGR2B* were induced to levels comparable to isolated primary human LSECs, the levels of *F8* were over 160-fold lower, suggesting that either LSEC-LCs are not fully mature or only a small subset of cells expresses the gene. Culture of isolated CD31⁺ LSEC-LCs for a further 10 days revealed that they maintained a stable expression pattern (data not shown). Although LSECs derive from venous vasculature, SB and cAMP also induced the expression of LSEC markers in arterial-angioblast-derived cells (Figures S2D and S2E). However, this specification required longer application of stimuli (4–8 total days) and higher cAMP

Figure 2. Effect of Hypoxia on LSEC-LC Specification

- (A) Schematic of LSEC-like cell (LSEC-LC) derivation from angioblasts under controlled oxygen levels.
 (B) Representative flow cytometric analysis of LYVE1 and CD32 expression on CD31⁺ cells under hypoxic (5% CO₂/5% O₂/90% N₂) and normoxic (5% CO₂/95% air) conditions.
 (C) Quantification of LYVE1⁺ CD32⁺ cell frequency as a percentage of total CD31⁺ arterial and venous cells from day 12 to 22 under hypoxic or normoxic culture (mean ± SEM, two-way ANOVA; *p < 0.05, ***p < 0.001 versus day 12 within oxygen tension and cell type; #p < 0.05, hypoxic artery versus hypoxic vein at the indicated day; §p < 0.05, hypoxia versus normoxia within a cell type at the indicated day).
 (D) qRT-PCR analysis of LSEC markers in the populations described and statistically assessed as in (C) (red line, primary LSEC expression).
 (E) qRT-PCR analysis of LSEC markers in isolated hypoxic arterial and venous CD31⁺ LSEC-LCs at days 15–18. Values are normalized to *TBP* (mean ± SEM, one-way ANOVA; *p < 0.05, **p < 0.01, ***p < 0.001, CD31⁺ versus CD31⁻ within cell type; ###p < 0.001, artery versus vein CD31⁺; red line, primary LSECs).
 (F and G) Immunofluorescence of LSEC markers in day 16 hypoxic arterial and venous LSEC-LCs with DAPI counterstain. (F) LYVE1, CD31, and CD32B expression in arterial and venous cells. (G) LYVE1, CD31, and STAB2 expression in arterial and venous cells. Scale bar represents 50 μm. **** indicates location of enlarged single-channel inset panels.
 (H) Flow cytometric analysis of AcLDL-AF488 or FSA-FITC binding (10 min, 37°C) in CD31⁺ arterial and venous endothelial cells (day 12) and LSEC-LCs (day 16) (mean ± SEM, one-way ANOVA, **p < 0.01, ***p < 0.001, as indicated).

dosing and was associated with increased *VWF* expression (Figures 2D, S2D, and S2E).

As the hepatic vasculature resides in distinct metabolic zones (1–3) that differ in oxygen content (Martinez et al., 2008), we hypothesized that oxygen tension could impact the development and maturation of hPSC-derived LSECs. To investigate this, we modeled oxygen zonation by culturing arterial and venous angioblasts under hypoxic (5% O₂) or normoxic (21% O₂) conditions from day 8 onward using CD32B/*FCGR2B* as an oxygen-sensitive readout of LSEC specification/zonation (MacParland et al., 2018; Strauss et al., 2017). SB and cAMP were added from day 12, and cells were assessed every 2 days between days 12 and 22 (Figure 2A). While oxygen tension did not impact CD34⁺CD31⁺ endothelial cell frequency (data not shown), hypoxic culture promoted the development of a CD31⁺LYVE1⁺CD32⁺ population from both the venous and arterial lineages (Figures 2B and 2C). Notably, this CD32B/*FCGR2B*⁺ population was induced 2–4 days earlier in venous cells than in arterial cells (Figures 2B–2D). qRT-PCR-based analyses of the total populations confirmed the differential upregulation of *FCGR2B* expression in the two populations and showed a dramatic hypoxia-induced increase in *STAB2* expression in the venous LSEC-LCs (Figure 2D). Molecular analyses of the isolated day 16 CD31⁺LYVE1⁺ LSEC-LC populations revealed that venous cells expressed significantly higher levels of *STAB2* and CD32B/*FCGR2B* than arterial cells. No differences were detected in the levels of *LYVE1*, *F8*, or *PLVAP* (Figure 2E). Immunocytochemistry analysis showed that venous LYVE1-positive LSEC-LCs expressed higher levels of CD32B and *STAB2* protein than arterial cells (Figures 2F and 2G). Venous LSEC-LCs also showed greater binding of acetylated low density lipoprotein (AcLDL) and formaldehyde-treated serum albumin (FSA) than arterial LSEC-LCs, indicating that elevated scavenger receptor expression is indicative of increased function (Figure 2H). Taken together, these data demonstrate that venous-angioblast-derived endothelial cells more rapidly and robustly upregulate LSEC markers and ligand-binding functions than arterial-derived endothelial cells when cultured in anatomically appropriate hypoxic stimuli.

To further investigate the role of oxygen on LSEC marker expression and identify a pharmacological means of enhancing CD32B expression, we next interrogated the hypoxia-inducible factor 1- α (HIF1 α) signaling pathway as a probable mechanistic regulator of endothelial cell (EC) gene expression. Application of IOX2, a specific prolyl hydroxylase (PHD) inhibitor that stabilizes HIF1 α , induced the upregulation of *FCGR2B* and *F8* expression and a downregulation of *LYVE1* expression in venous and arterial ECs cultured under normoxic conditions (Figure S3B). The expression levels of *STAB2* levels were not impacted by IOX2. Flow cytometric analyses confirmed that under hypoxic or normoxic conditions IOX2 induced the development of CD31⁺LYVE1⁺CD32⁺ cells in both populations (Figure S3C). Venous cells were more sensitive than arterial cells to HIF1 α stabilization, resulting in endothelial populations consisting of >95% LYVE1⁺CD32⁺ cells. These results reinforce the differences in response between artery and venous cells and that more extreme hypoxic signaling (hypoxic culture with IOX2 addition) is unable to uniformly convert arterial cells to a CD32⁺ phenotype.

Transplantation of Angioblasts and Endothelial Cells

To determine if an *in vivo* environment would support the development of bona fide *F8*-expressing LSECs, we next transplanted day 8 CD34⁺ angioblasts or day 14–16 CD31⁺ LSEC-LCs into the liver of 1- to 4-day-old irradiated neonatal NOD *scid* gamma (NSG) mice. To facilitate identification and recovery of human-derived cells, the populations used for these transplantation experiments were generated from HES2-tRFP human ESCs (hESCs) (Irion et al., 2007). Analyses of the frequency of RFP⁺ cells within the non-parenchymal cell (NPC) fraction of the recipient livers revealed that all hPSC-derived cell populations displayed some capacity to engraft the neonatal liver (Figure 3A). Defining 1% RFP⁺ cells in the NPC as a positive response, we found that 47.4% of the venous angioblast recipients, 12.5% of the arterial angioblast recipients, 16.7% of the venous LSEC-LC recipients, and 9.1% of the arterial LSEC-LC recipients were engrafted (Figure 3B). In contrast, human umbilical vein endothelial cells (HUVECs), representing mature venous endothelial cells, showed no capacity to stably engraft NSG livers (<0.001% CD31⁺, n = 5 at 73–80 days post-transplant). All RFP⁺ grafts had a CD31⁺ population that contained CD32⁺LYVE1⁺, CD32⁺LYVE1⁻, and CD32⁻LYVE1⁻ subpopulations. CD31⁻ cells were also detected in all grafts. Comparative analyses revealed that the venous angioblasts consistently generated the largest CD31⁺ endothelial population (62% \pm 4% of tRFP⁺) and the largest CD32⁺LYVE1⁺ (53% \pm 3% of RFP⁺CD31⁺) LSEC-like subpopulation (Figures 3C and 3D).

Molecular analysis of different fractions isolated from venous-angioblast-derived grafts showed that the CD31⁺CD32⁺LYVE1⁺ cells expressed higher levels of the LSEC markers *LYVE1*, *STAB2*, *FCGR2B*, *F8*, *CD14*, *MRC1*, *RAMP3*, *PLVAP*, *CD36*, and *GATA4* and lower levels of the general endothelial markers *PECAM1*, *VWF*, and *CALCRL* than either the CD31⁺CD32⁻LYVE1⁻ cells or the other populations (Figure 3E). Many of the markers were expressed at levels as high as or higher than those detected in primary isolated LSECs (Figure S4). Notably, the levels of *F8* expression (8 \pm 1 *F8/TBP*) were 80-fold above those in the LSEC-LCs generated *in vitro* (0.1 \pm 0.02 *F8/TBP*) and ~50% of those in the isolated primary LSEC levels (13 \pm 4 *F8/TBP*). These expression profiles support the interpretation that CD31⁺CD32⁺LYVE1⁺ cells represent human LSECs. CD31⁺CD32⁺LYVE1⁻ cells expressed lower levels of LSEC markers, suggesting they may represent a less mature endothelial population or a transitional sinusoidal zone LSEC population. The RFP⁺CD31⁻ cells observed in neonatal transplants expressed *ACTA2*, *PDGFRB*, *DDR2*, and *MGP* but none of the LSEC markers, indicating they represent mesenchymal/fibroblast cells similar to the *in vitro* CD31⁻PDGFR β ⁺ cells. Using the CD31⁺CD32⁺LYVE1⁺ phenotype as a measure of LSECs, we calculated the frequency of these cells (percentage of live NPC) in each transplant and found that venous angioblasts were most efficient at generating human LSECs in the neonatal model (Figure 3F).

To further investigate the *in vivo* potential of the hPSC-derived LSEC progenitors, we next transplanted the venous and arterial angioblasts into adult NSG mice conditioned with 150 mg/kg monocrotaline to induce vascular injury (Deleve, 2013a; Filali et al., 2013). Although both populations showed engraftment (>1% of NPCs), venous angioblasts generated substantially higher levels of total RFP⁺ cells (venous: 44.2% \pm 8% RFP⁺

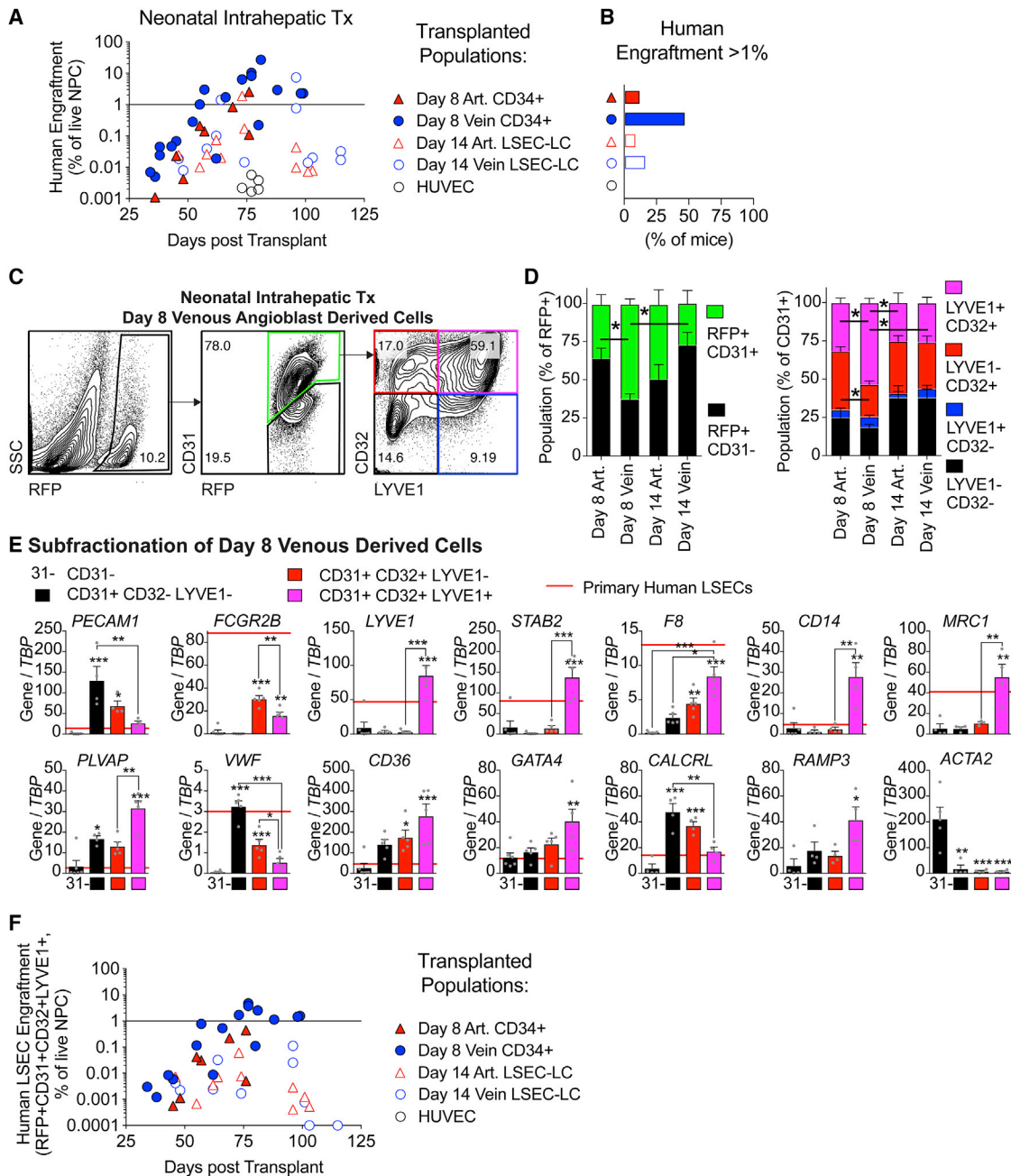


Figure 3. Engraftment of hPSC-Derived Angioblasts and LSEC-LCs in Neonatal NSG Mice

(A) Engraftment potential (RFP⁺ % non-parenchymal cells [NPCs]) of venous and arterial angioblasts (day 8, CD34⁺), LSEC-LCs (day 14–16, CD31⁺), and human umbilical vein endothelial cells (HUVECs) (CD31⁺ % NPCs) within the liver NPC population following neonatal engraftment.

(B) Frequency of mice (from A) with >1% human RFP⁺. Neonatal Transplant (Tx), day 8 CD34⁺ Artery (Art.) n = 1/8; day 8 CD34⁺ Vein n = 9/19; day 14–16 CD31⁺ Art. LSEC-LC n = 1/11; day 14–16 CD31⁺ Vein LSEC-LC n = 2/12.

(C) Flow cytometric analysis of NPC populations generated from day 8 venous angioblasts 77 days post-transplantation.

(D) Quantification of RFP⁺ NPC subpopulations in grafts from arterial or venous angioblasts or LSEC-LCs (mean ± SEM, two-way ANOVA; *p < 0.05, as indicated; n = 7–21 mice per transplant group).

(E) qRT-PCR analysis of LSEC markers in FACS-isolated CD31⁺, CD32⁺, and LYVE1⁺ NPC subpopulations derived from venous angioblasts 45–80 days post-transplant. Values are normalized to *TBP* (mean ± SEM, one-way ANOVA; *p < 0.05, **p < 0.01, ***p < 0.001 versus RFP⁺ CD31⁻ cells and as indicated; red line, primary LSECs).

(F) Quantification of LSEC engraftment (% RFP⁺ CD31⁺CD32⁺LYVE1⁺ of NPCs) from transplanted populations at the indicated times.

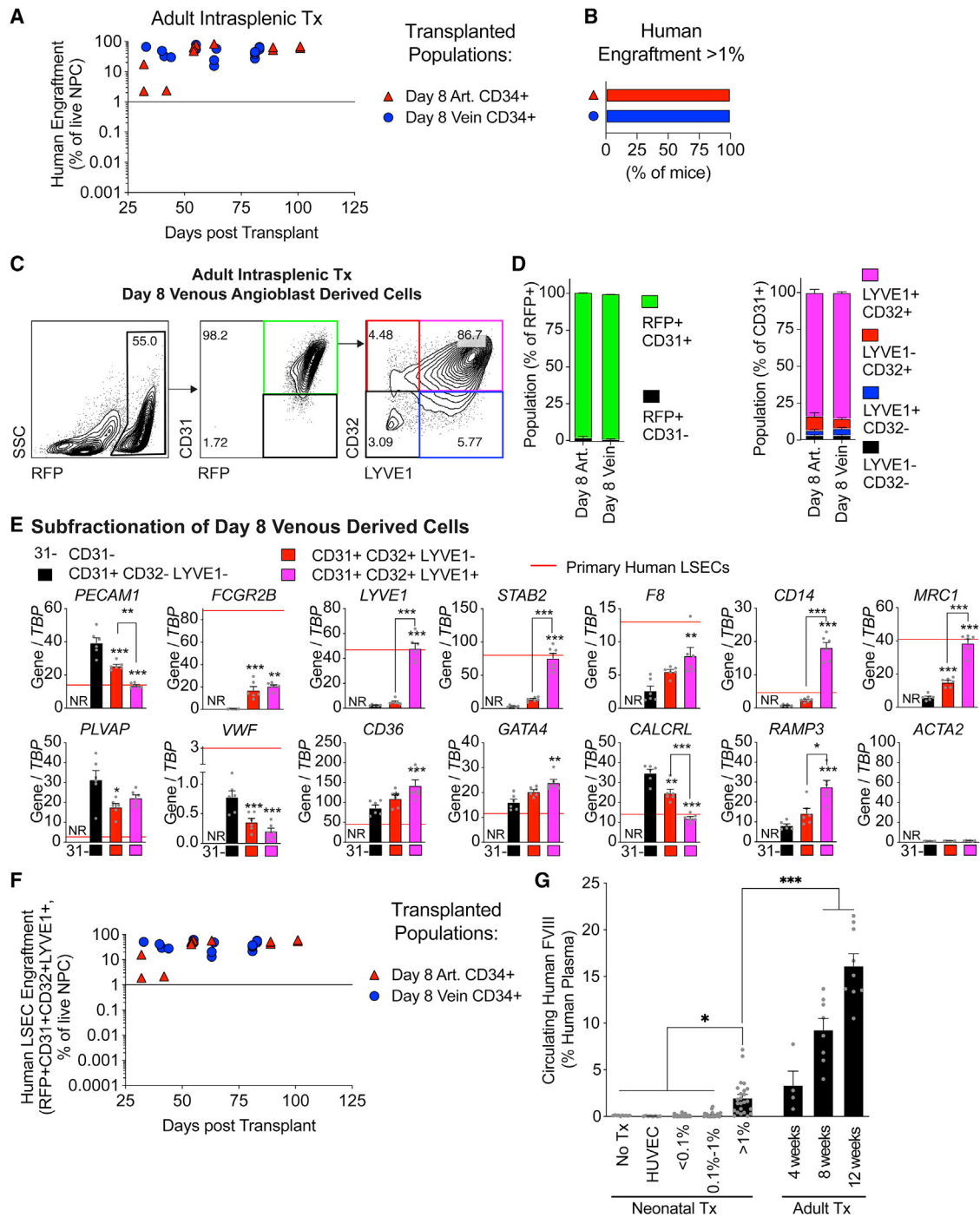


Figure 4. Engraftment of hPSC-Derived Angioblasts in Adult NSG Mice

(A) Engraftment of venous and arterial angioblasts (day 8, CD34⁺) within liver NPCs at the indicated days following transplantation into adult NSG mice.

(B) Frequency of mice (from A) with >1% human RFP⁺. Adult Tx: day 8 CD34⁺ Art. n = 12/12; day 8 CD34⁺ Vein n = 18/18.

(C) Flow cytometric analysis of NPC populations generated from day 8 venous angioblasts 55 days post-transplantation.

(D) Quantification of RFP⁺ NPC subpopulations in grafts from arterial or venous angioblasts (mean ± SEM, n = 8–15 mice per transplant group).

(E) qRT-PCR analysis of LSEC markers in FACS-isolated CD31⁺, CD32⁺, and LYVE1⁺ NPC subpopulations derived from venous angioblasts 55–83 days post-transplant. Values are normalized to *TBP* (mean ± SEM, one-way ANOVA; *p < 0.05, **p < 0.01, ***p < 0.001 versus RFP⁺ CD31⁺CD32⁺LYVE1⁺ cells and as indicated; red line, primary LSECs; NR indicates not recoverable RFP⁺ CD31⁺ cells).

(F) Quantification of LSEC engraftment (% RFP⁺ CD31⁺CD32⁺LYVE1⁺ of NPCs) from transplanted angioblasts at the indicated times.

(legend continued on next page)

[% NPCs]; arterial: $7.4\% \pm 5\%$; $p = 0.0185$, $n = 3-4$) and $CD31^+CD32^+LYVE1^+$ LSECs (venous: $37.4\% \pm 6\%$ $RFP^+CD31^+CD32^+LYVE1^+$ [% NPCs]; arterial: $6.6\% \pm 4\%$; $p = 0.0096$, $n = 3-4$) than arterial angioblasts at the early stages of engraftment (days 32–44 days post-transplant) (Figures 4A, 4B, and 4F). Beyond 50 days, engraftment levels from both angioblast populations equalized (venous: $48\% \pm 4\%$ RFP^+ [% NPCs]; arterial: $50 \pm 8\%$; $n = 12-18$). The venous- and arterial-derived grafts at these later time points contained similar proportions of $CD31^+CD32^+LYVE1^+$ (% NPCs) LSECs (venous: $41\% \pm 3\%$; arterial: $41\% \pm 6\%$; $n = 12-18$) (Figure 4F). In contrast to the neonatal grafts, the majority of the cells in the adult liver grafts displayed the $CD31^+CD32^+LYVE1^+$ LSEC phenotype (venous: $86\% \pm 0.7\%$ $CD32^+LYVE1^+$ [% RFP^+CD31^+]; arterial: $84\% \pm 2.3\%$; $n = 12-18$) (Figures 4C and 4D). Molecular analyses of this population showed that it displayed a gene expression profile indicative of functional human LSECs, similar to the cells in the grafts generated in the neonatal model (Figure 4E). Collectively, these findings demonstrate that it is possible to generate hPSC-derived LSECs in the liver *in vivo* and suggest that the adult injured liver provides a more supportive environment than the neonatal liver for the development of this lineage.

As mature functional LSECs secrete FVIII, we next analyzed the plasma of the transplanted animals for the presence of this coagulation factor. Neonatally transplanted animals with $>1\%$ RFP^+ NPCs contained low but detectable levels of circulating human FVIII (Figure 4G). No FVIII was detected in animals with smaller grafts ($<1\%$), in animals transplanted with HUVECs or untransplanted controls. Analyses of adult animals transplanted with venous-angioblast-derived grafts showed an increase in the amount of FVIII over time, reaching levels of 16% ($16.1\% \pm 1.3\%$; $n = 9$) of those in normal human plasma at 12 weeks following transplantation. These observations demonstrate that hPSC-derived LSECs are functional and able to produce and secrete FVIII at levels that are considered to be therapeutically relevant.

Histological examination of the livers of mice transplanted venous angioblasts by either method revealed the presence of readily detectable human $KU80^+$ grafts (Figures 5 and S5). Neonatal grafts were focal and often associated with central veins and surrounding pericentral zone 2/3 sinusoids (Figures 5A–5E), while adult grafts were more broadly distributed (Figure 5F–5J). The pericentral engrafted regions contained $KU80^+$ human cells that expressed human specific $CD31$, $CD32B$, $LYVE1$, $STAB2$, $GATA4$, and $FVIII$ proteins indicative of properly zoned human LSEC engraftment within the sinusoidal environment (Figures 5A–5N). The hPSC-derived LSECs were found situated in close contact with the mouse hepatocytes and intraluminal $F4/80$ -positive macrophages/Kupffer cells (Figure 5O). Engraftment was also observed in the periportal sinusoids (zone 1), as demonstrated by the presence of $KU80^+CD31^{low}$ cells that lacked expression of $LYVE1$, $CD32B$, and $STAB2$ (Figure S5F). In addition to LSECs, $KU80^+$ portal capillaries that expressed high levels of $CD31$ and $CD34$ but little (if any) $LYVE1$, $CD32B$, and $STAB2$ were detected adjacent to bile ducts (Figures 5P and S5F). Most

neonatal grafts also had collagen-rich nodular structures that contained $KU80^+CD31^-$ cells that expressed smooth muscle actin and vimentin (Figures S5A–S5E). These structures were rarely detected in the adult grafted animals. Together, these findings demonstrate that the venous angioblast population is able to engraft the pericentral and midlobular sinusoids of the liver to generate functional LSECs. Additionally, these progenitors display potential to engraft the periportal sinusoids and portal triad microvasculature.

scRNA-Seq Analysis of Engrafted Cells

To further characterize the molecular makeup of the hPSC-derived grafts, we carried out single-cell RNA sequencing (scRNA-seq) analyses on the whole RFP^+ NPC fraction isolated from a venous-derived neonatal graft (Table S1). Of the 5,951 RFP^+ cells profiled, 5,258 (88.4%) were $PECAM1^+$ endothelial cells (clusters 0, 1, and 3), and the remaining 693 (11.6%) were $PECAM1^-$ cells (clusters 2 and 4) (Figure 6A). Differential gene expression analysis between clusters (Table S2) showed that cluster 0 (64% of RFP^+) was defined by high expression of scavenger receptors ($LYVE1$, $STAB1$, $STAB2$, $FCGR2B$, $CD14$, and $MRC1$), secreted products such as $F8$, and other markers of the LSEC lineage ($DNASE1L1$, $CLEC1B$, and $RAMP3$) (Figures 6B and S6). These cells did not express VWF and showed lower levels of the canonical vascular markers $PECAM1$ and $CD34$ compared to cells in cluster 1. This expression pattern closely matches that of $RFP^+CD31^{+low}CD32^+LYVE1^+$ cells isolated from mice (Figures 3E and 4E) and $LYVE1^+CD32B^+MRC1^+STAB2^+GATA4^+FVIII^+$ cells observed lining the pericentral and midlobular sinusoids of the grafts (Figure 5). The second largest endothelial cluster (1,005 cells, 17% of RFP^+ cells), cluster 1, had little to no expression of the scavenger genes observed in cluster 0 but instead had elevated expression of $PECAM1$, $CD34$, $PLVAP$, and VWF in a subset of cells. This pattern is similar to that of the $RFP^+CD31^+CD32^-LYVE1^-$ population isolated from the graft (Figure 3E and 4E) and is indicative of a mixture of $CD31^{low}CD32^-LYVE1^-$ periportal sinusoidal cells and $CD34^{high}CD31^{high}CD32^-LYVE1^-$ portal-associated microvasculature observed in our histological analyses (Figures 5P and S5F). Cluster 3 consists of 452 cells (7.6% of RFP^+) that were annotated as proliferating LSECs given their high G2/M cell cycle score and expression of $PECAM1$, $MKI67$, $CDK1$, $CDKN3$, $PCNA$, $CCNB1$, and $ID1$ as well as $LYVE1$, $STAB2$, and $MRC1$ (Figures 6B and S6). Cluster 2 (592 cells; 10%) and 4 (101 cells; 1.7%) represent $RFP^+PECAM1^-$ cells that express multiple collagens, $ACTA2$, VIM , $PDGFRB$, $DDR2$, $POSTN$, $TGFB1$, DES , and other genes indicative of a fibroblast/mesenchymal lineage (Figures 6B and S6). These cells may be similar to the isolated RFP^+CD31^- cells (Figure 3E) and the $SMA^+VIM^+COL1^+COL3^+$ cells in the nodules of the grafts (Figures 3E and S5A–S5E).

We next compared these expression patterns to those identified from primary human liver scRNA-seq analyses (MacParland et al., 2018) by integration following batch correction with Harmony (Korsunsky et al., 2019) (Figure 6C). These analyses revealed that the

(G) Plasma levels of human-specific FVIII antigen levels (% normal human plasma) in NSG mice transplanted with indicated cell types (neonatal: 45–112 days post-transplant; adults: days 33–101 post-transplant). Neonatal samples include nontransplanted mice, and mice transplanted with HUVECs or hPSC-derived cells (all populations) grouped by engraftment level. Adult transplant samples are mice transplanted with venous angioblasts at the indicated times (mean \pm SEM, one-way ANOVA, * $p < 0.05$, *** $p < 0.001$, as indicated).

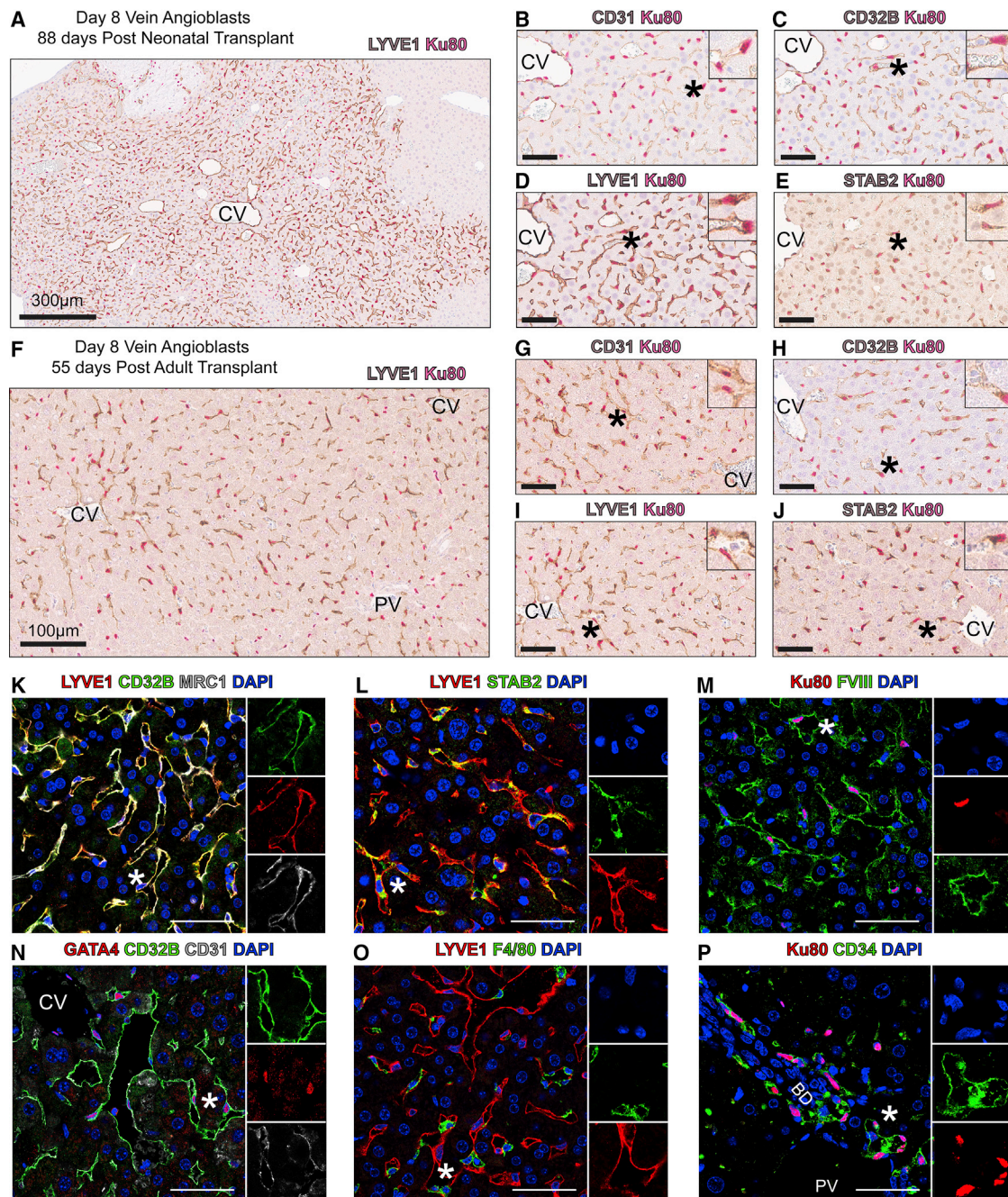


Figure 5. Histological Characterization of Engrafting Endothelial Cells

(A–J) Histological analysis of livers from mice engrafted with venous angioblasts (A–E; neonatal 88 days post-transplant; F–J; adult 55 days post-transplant). Sections were analyzed with human-specific endothelial/LSEC markers (CD31, LYVE1, CD32B, and STAB2) and the human-specific nuclear antigen Ku80. LYVE1 and Ku80 expression (A, D, F, and I), CD31 and Ku80 expression (B and G), CD32B and Ku80 expression (C and H), and STAB2 and Ku80 expression (E and J) are depicted. “*” indicates location of enlarged inset panels; scale bars represent 60 μm unless otherwise indicated.

(K–P) Immunofluorescence analyses of liver samples (vein-angioblast-derived grafts 33–88 days post-transplant) from neonatal (K, M, and N) and adult (L, O, and P) transplant models stained for LSEC and endothelial markers, mouse macrophage marker F4/80, and counterstained with DAPI. (K) LYVE1, CD32B and MRC1 expression. (L) LYVE1 and STAB2 expression. (M) Ku80 and human FVIII expression. (N) GATA4, CD32B, and CD31 expression. (O) LYVE1 and mouse F4/80 expression. (P) Ku80 and CD34 expression neighbouring a bile duct. “*” indicates location of enlarged single-channel inset panels as indicated; scale bar represents 50 μm . The central vein (CV), portal vein (PV) and bile duct (BD) are indicated.

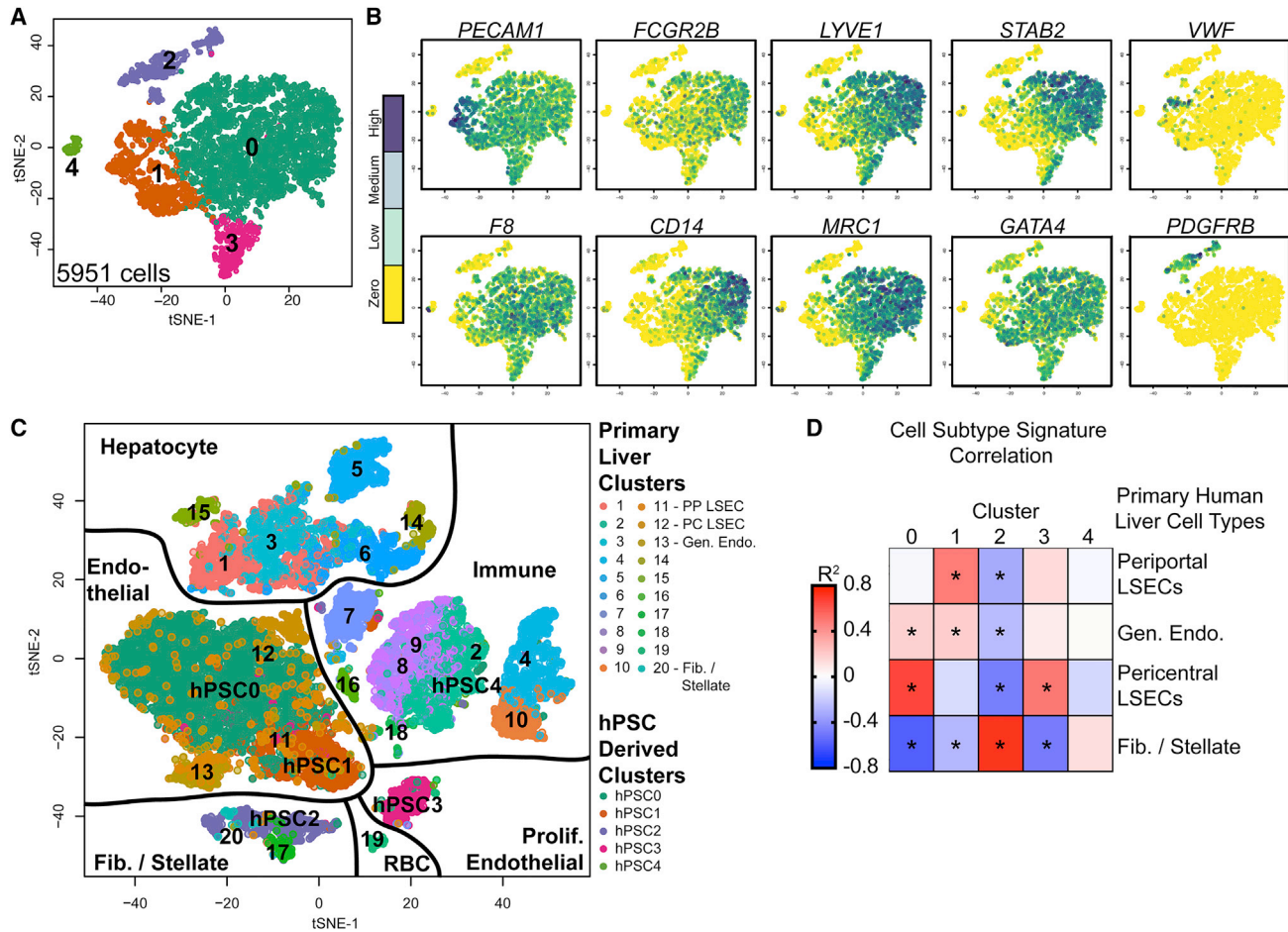


Figure 6. scRNA-Seq Analyses of hPSC Venous-Angioblast-Derived Populations

Analyses of venous-angioblast-derived DAPI⁺ RFP⁺ cells isolated 77 days after neonatal transplant.

(A) t-distributed stochastic neighbor embedding (t-SNE) projection of 5,951 filtered hPSC-derived cells segmented into five clusters (clusters 0–4).

(B) Candidate expression patterns of markers of LSECs (*PECAM1*, *FCGR2B*, *LYVE1*, *STAB2*, *F8*, *CD14*, *MRC1*, and *GATA4*), general vasculature (*PECAM1* and *VWF*), and mesenchyme/fibroblasts (*PDGFRB*).

(C) t-SNE projection of Harmony integration of 20 primary human liver cell types (clusters 1–20 as described by MacParland et al., 2018) and hPSC-derived cells (hPSC clusters 0–4 as described in A). Primary liver cell populations include hepatocytes (14, 5, 6, 3, 1, and 15), immune cells (B cells: 7 and 16; natural killer [NK] cells: 8; T cells: 2, 9, and 18; and macrophages: 10 and 4), fibroblast/stellate cells (20), cholangiocytes (17), and red blood cells (RBCs) (19).

(D) Pearson correlation analysis between hPSC-derived clusters and primary liver clusters using differentially expressed hepatic-, endothelial-, and stellate/fibroblast-cell-specific signature genes (Table S3). R² values are depicted as a heatmap (positive correlation, red; negative correlation, blue), with significant correlations indicated (*p < 0.05). User-friendly interactive data visualization of hPSC-derived and Harmonized human liver scRNA-seq data can be explored via scClustViz (Innes and Bader, 2018) at http://shiny.baderlab.org/hPSC_LSECsAndHumanLiver/.

nonproliferating hPSC-derived endothelial cells (hPSC clusters hPSC0 and hPSC1) closely associated with the liver endothelium containing periportal LSECs (11), pericentral LSECs (12), and general endothelium (13). Indeed, 98% of hPSC0 cells and 83% of hPSC1 cells were contained within this human liver endothelium defined region suggesting transcriptional similarity between these endothelial populations. The majority (94%) of cells from cluster hPSC2 grouped with liver stellate/fibroblasts (cluster 20) and rare cholangiocytes suggesting a fibroblast identity. Cluster hPSC3, the proliferating LSECs, grouped poorly with any resident liver cell type presumably due to the low abundance of proliferating endothelial cells in the non-diseased adult human liver. Cluster hPSC4, integrated within the immune cell clusters of the human liver data, split between macrophages (43%) and T cells (45%).

To quantify the similarity between the hPSC-derived cells and primary liver endothelial cells and fibroblasts, we selected the 50 most differentially expressed genes that identified each of the 20 human liver cell types (Table S3). Using the genes that defined liver-derived fibroblasts/stellate cells, general endothelium, pericentral LSECs (zone 2/3), and periportal LSECs (zone 1), we performed Pearson correlation analyses with our clusters (Figure 6D). These analyses showed that hPSC cluster 0 positively correlated to pericentral zone 2/3 human LSECs (R² = 0.65, p = 7e–19), but not to periportal zone 1 human LSECs (R² = –0.03, p = 0.7). hPSC cluster 1 correlated to periportal zone 1 LSECs (R² = 0.48, p = 1e–9) and general endothelial cells (R² = 0.18, p = 3e–2), but not to pericentral zone 2/3 human LSECs (R² = –0.14, p = 9e–2). Cluster 3 correlated to pericentral

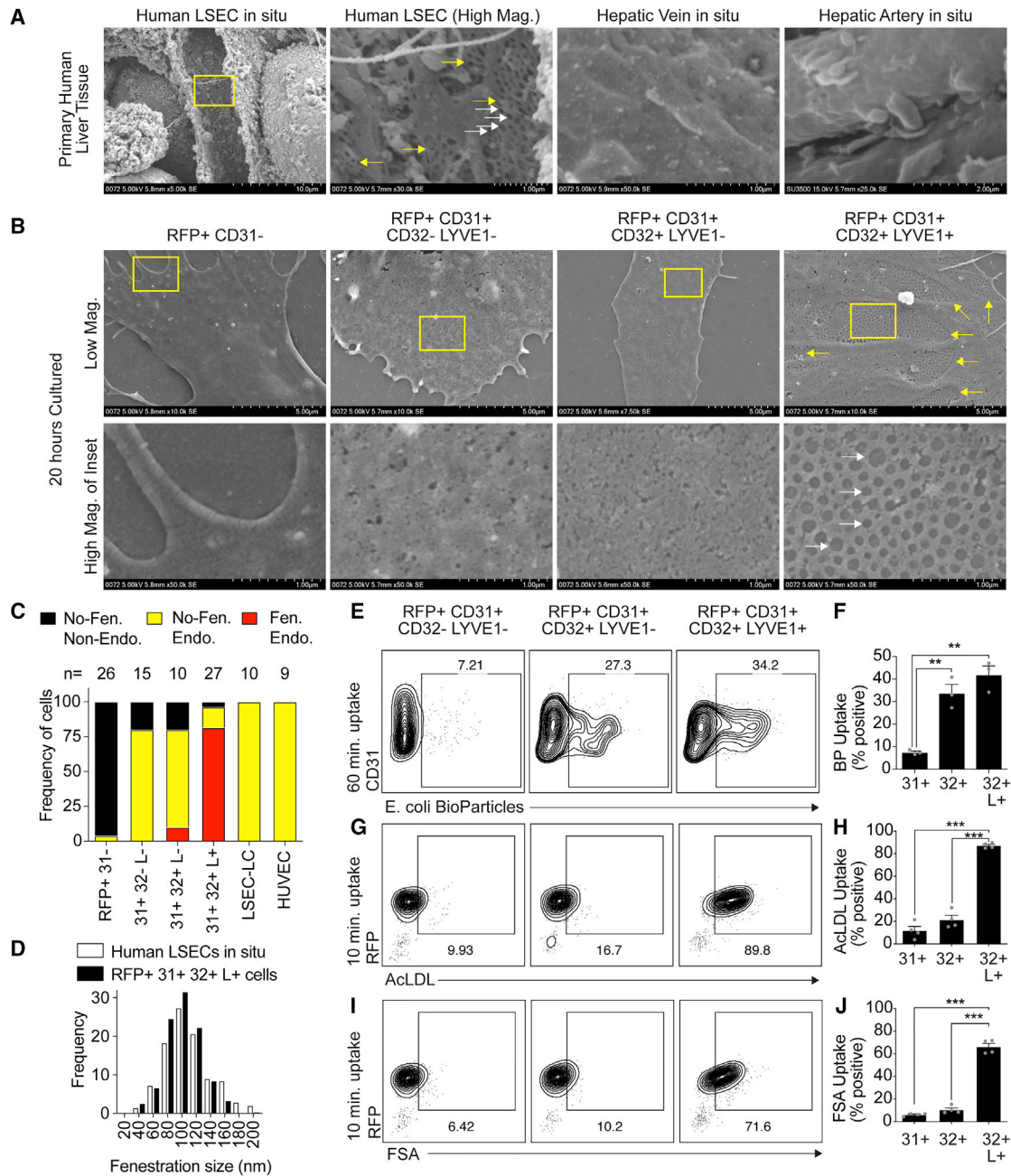


Figure 7. Analyses of Fenestrations and Scavenging Potential of hPSC-Derived LSECs

(A and B) Scanning electron microscopic images of primary human *in situ* LSECs, hepatic venous and arterial endothelium, and isolated hPSC-derived populations from venous angioblast engrafted livers (38–77 days). (A) Primary liver tissue with LSEC in sinusoid under low magnification (left) and higher magnification (middle left), and high magnification of hepatic vein (middle right), and hepatic artery (right). (B) Indicated FACS isolated hPSC-derived populations under low (top) and high (bottom) magnifications. Higher-magnification image (yellow box area in low magnification) depicts fenestrations (white arrows) arranged in sieve plates (yellow arrows) in CD31⁺CD32⁺LYVE1⁺ cells and primary LSECs. Scale bars as indicated below images.

(C) Frequency of fenestrated cells (>10 fenestrations in a sieve plate), endothelial cells (smooth-edged cells with angiogenic lateral sprouts), and non-endothelial cells (fibroblast-like cells and rounded cells) was performed manually on the indicated numbers of cells (four or more independent experiments). *In vitro*-derived venous LSEC-LCs and multi-donor-derived HUVECs were assessed alongside the graft-derived populations.

(D) Fenestration size (longest diameter) in primary human LSECs *in situ* (n = 5 cells, white) and venous-angioblast-derived LSECs (n = 8 cells, black).

(E–J) Flow cytometric analysis (E, G, and I) and quantification (F, H, and J) of ligand binding in indicated venous-angioblast-derived populations 72–99 days post-transplantation. (E and F) *E. coli* bioparticle binding in the presence of human immunoglobulin G (IgG) (60 min, 37°C). (G and H) AcLDL-AF488 binding (10 min, 37°C). (I and J) FITC-conjugated formaldehyde fixed serum albumin (FSA) binding (10 min, 37°C) (mean ± SEM, one-way ANOVA; **p < 0.01, ***p < 0.001, as indicated).

LSECs ($R^2 = 0.49$, $p = 4e-10$) matching the predicted identity as a LSEC proliferative cluster. hPSC cluster 2 positively correlated to fibroblast/stellate cells ($R^2 = 0.71$, $p = 1e-23$) and negatively correlated to all three endothelial clusters. As expected, hPSC cluster 4 did not significantly correlate to any comparators, likely due to the small number of cells and the suggested hematopoietic lineage relationship revealed by Harmony integration (Figure 6C). Taken together, the findings from these molecular analyses demonstrate that the hPSC-derived LSEC population generated *in vivo* shows molecular profiles similar to LSECs isolated from primary adult liver tissue.

Functional Characterization of Engrafted Cells

A key functional characteristic of mature LSECs is the presence of transcellular fenestrations clustered in sieve plates (Braet and Wisse, 2002; DeLeve, 2013b). Scanning electron microscopy analyses of primary liver tissue revealed the presence of such fenestrations in LSECs, but not in the portal vein or hepatic artery endothelium (Figure 7A), as expected. The RFP⁺CD31⁺CD32⁺LYVE1⁺ cells isolated from engrafted livers (neonatal) also showed abundant fenestrations that were arranged in well-defined sieve plates (Figures 7B and 7C). These fenestrations covered $\sim 6.5\% \pm 2.4\%$ of the cell surface area and ranged in size from 90 to 110 nm, similar to primary human LSECs (Figure 7D) (Braet and Wisse, 2002; Horn et al., 1987). Fenestrations were not detected in the RFP⁺CD31⁻ fibroblasts or in RFP⁺CD31⁺CD32⁻LYVE1⁻ cells and rarely in RFP⁺CD31⁺CD32⁺LYVE1⁻ cells. Similarly, fenestrations were not observed in HUVECs or *in vitro*-derived venous LSEC-LCs.

To further assess LSEC function, *in vivo*-matured, fluorescence-activated cell sorting (FACS)-isolated cells were treated with opsonized *E. coli* bioparticles (Ganesan et al., 2012; Mousavi et al., 2007), AcLDL, or FSA (Elvevold et al., 2008a; Nonaka et al., 2007; Xie et al., 2010). While both CD32⁺ fractions were readily able to bind bioparticles, only the CD31⁺CD32⁺LYVE1⁺ cells were able to bind all functional ligands (Figures 7E–7J). The general endothelial cells (CD31⁺CD32⁻LYVE1⁻) showed little capacity to bind the bioparticles or the ligands.

Collectively, the findings from these experiments demonstrate that the hPSC-derived LSECs display key characteristics and functional properties of adult liver LSECs, including the presence of fenestrations and functional scavenger receptors.

Generation of LSECs from H1-GFP hPSCs

To determine if this approach to generate LSECs is applicable to other hPSC lines, we generated venous angioblasts from H1-GFP hPSCs and transplanted them into neonatal mice. As shown in Figure S7, modulation of VEGF-A and Notch pathways facilitated arteriovenous angioblast and LSEC-LC specification of H1-GFP-derived cells (Figures S7B and S7C). Following neonatal transplantation, H1-GFP-derived venous angioblasts generated CD31⁺CD32⁺LYVE1⁺ populations (Figures S7D–S7G) that displayed the LSEC molecular signature and fenestration patterns observed in HES2-derived cells (Figures S7H and S7I).

DISCUSSION

The successful derivation of functional cells from hPSCs relies on our understanding of the regulatory pathways that control devel-

opment of the corresponding cell type in the early embryo. With respect to LSECs, studies in different model organisms have provided strong evidence that these cells derive from sinus venosus and hepatic portal-derived venous vasculature (Hen et al., 2015; Zhang et al., 2016) and that their development is regulated in part by TGF- β and adrenomedullin/RAMP signaling (Arai et al., 2011; Ichikawa-Shindo et al., 2008; Kouji et al., 2017; Koyama et al., 2013; Nonaka et al., 2008; Shindo et al., 2001). In this study, we recapitulate these developmental events in hPSC-differentiation cultures and show that venous angioblasts respond to cAMP, hypoxia, and low TGF- β signaling to upregulate the expression of mature LSEC markers. Engraftment in the liver of newborn and adult mice promoted maturation of the hPSC-derived angioblasts to endothelial cells that display many hallmarks of adult LSECs, including sinusoidal localization; gene expression patterns; the presence of fenestrations arranged in sieve plates; the capacity to scavenge *E. coli* bioparticles, AcLDL, and FSA; and the ability to secrete FVIII. Together, these findings reinforce the importance of understanding and applying both developmental and anatomical signaling cues to generate fully mature, functional hPSC-derived cell types.

Our observation that arterial and venous angioblast specification is sensitive to VEGF-A and Notch signaling dosage is consistent with previous studies (Ditadi et al., 2015; Prasain et al., 2014; Sriram et al., 2015; Zhang et al., 2017) and provides a simple means to regulate arteriovenous development in bulk cultures. Similarly, our observation that cAMP agonism and TGF- β inhibition upregulate LSEC markers (*LYVE1*, *STAB2*, *FCGR2B*, and *F8*) in both arterial and venous endothelial cells is in line with previous studies using PSC-derived endothelial cell populations of undetermined arterial or venous identity (Arai et al., 2011; Kouji et al., 2017; Nonaka et al., 2008). Although both angioblast populations responded to cAMP and TGF- β inhibition, venous cells showed accelerated upregulation of *FCGR2B/CD32B* expression and higher expression of *STAB2* than arterial cells in response to hypoxia or IOX2. This rapid and robust sensitized hypoxia/HIF1 α response by venous cells matches the predicted contribution of venous endothelium to the hypoxic portal vein, sinusoid, and central vein compartments. Furthermore, the decreasing oxygen gradient from hepatic zones 1–3 that is associated with elevated CD32B expression (MacParland et al., 2018; Strauss et al., 2017) is mirrored by the IOX2 dose-dependent induction of *FCGR2B/CD32B* in LSEC-LCs.

Our *in vivo* studies show that hPSC-derived angioblasts can engraft the liver in both the neonatal and adult transplant models and respond to the organ microenvironmental cues to generate functional LSECs that display molecular profiles similar to LSECs isolated from healthy primary tissue. The observation that HUVECs failed to engraft and that venous angioblasts engraft more efficiently than arterial angioblasts indicates that not all endothelial lineage cells display the same potential to generate LSECs *in vivo*. Additionally, the differences between the venous and arterial cells that we observed is consistent with the lineage-tracing studies in mice and fish (Hen et al., 2015; Zhang et al., 2016), showing that LSECs preferentially derive from the venous vasculature. Although both transplant models supported LSEC development, engraftment was quicker and LSEC differentiation was more efficient in adults. The efficiency in the adult model yielded grafts that comprised $\sim 40\%$ of the non-parenchymal

liver fraction and consisted of >80% CD31⁺CD32⁺LYVE1⁺ cells (LSEC phenotype). With this approach, it is possible to generate 8–12 million human LSECs per mouse within 1 month of transplantation, providing ready access to these cells for *in vitro* and *in vivo* studies.

As LSECs have been established as a therapeutically relevant source of FVIII *in vivo* (Fomin et al., 2013; Shahani et al., 2014), replacement of this population through cell-based therapy is one approach to treat hemophilia A. Support for this concept comes from the demonstration that hemophilia A mice could be treated by transplantation with primary LSECs (Follenzi et al., 2008) and that human-fetal-liver-derived endothelial cells could engraft, mature, and secrete therapeutic levels of FVIII in urokinase-type plasminogen activator (uPA)-NOG mice (Fomin et al., 2013). The potential of hPSC-derived cells to treat hemophilia A has been documented by Olgasi et al. who showed that iPSC-derived endothelial cells transduced with a F8 expressing lentivirus produced therapeutic levels of the factor (~6% hFVIII activity) when transplanted into NSG-HA hemophilic mice (Olgasi et al., 2018). This amount of FVIII was sufficient to correct the bleeding phenotype in these animals. The adult recipients in our study showed FVIII levels of up to 16% of normal human levels. If translatable to humans, this level of FVIII protein would be therapeutically relevant for patients with severe hemophilia A who produce less than 1% FVIII (Blanchette et al., 2014; Srivastava et al., 2013; White et al., 2001).

In addition to adult molecular profiles, hPSC-derived CD31⁺CD32⁺LYVE1⁺ cells displayed functional attributes of adult LSECs, including fenestrations organized in sieve plates and the ability to scavenge *E. coli*, AcLDL, and FSA. LSEC fenestrations normally function *in vivo* to regulate the movement of lipoproteins and dissolved metabolites from blood to hepatocytes through tightly regulated dilatation and constriction responses (Braet and Wisse, 2002). LSEC scavenging to sequester a number of ligands from the blood remains a hallmark function of these cells within the liver (Elvevold et al., 2004, 2008b). The fact that our fenestrated, ligand-binding hPSC-derived LSECs display these characteristics provides an opportunity to better understand the mechanisms that regulate human LSEC functions in normal and diseased states modeled in NSG mice.

Beyond a source of cells for therapy, our current hPSC-derived venous angioblast transplantation systems that humanize the hepatic vasculature and generate recoverable mature human LSECs provides a new experimental approach to investigate the developmental origins of these cells and the pathways that control their specification and maturation. Being amenable to *in vitro* genetic perturbations and toxicology studies, this model offers many new avenues to explore the role of LSECs in normal liver function and human disease. Finally, while LSECs represent one example of a disease-relevant organ-specific endothelial bed, the application of this experimental approach to other organs offers an exciting opportunity to understand the developmental and anatomical factors that regulate unique organ vasculature specialization beyond the liver.

STAR★METHODS

Detailed methods are provided in the online version of this paper and include the following:

- KEY RESOURCES TABLE
- RESOURCE AVAILABILITY
 - Lead Contact
 - Materials Availability
 - Data and Code Availability
- EXPERIMENTAL MODEL AND SUBJECT DETAILS
 - Animals
 - Cell Lines
 - Primary Cell Cultures
- METHOD DETAILS
 - Directed Differentiation of Angioblasts from hESCs
 - Angioblast Specification and LSEC Marker Induction
 - Flow Cytometry and FACS
 - Quantitative Reverse Transcription PCR
 - Neonatal Intrahepatic Transplantation
 - Adult Intrasplenic Transplantation
 - Non-Parenchymal Cell Isolation and *ex vivo* Analysis
 - Scanning Electron Microscopy of Fenestrations
 - Immunohistochemistry and Immunofluorescence
 - Single-Cell RNA-seq Analysis
- QUANTIFICATION AND STATISTICAL ANALYSIS

SUPPLEMENTAL INFORMATION

Supplemental Information can be found online at <https://doi.org/10.1016/j.stem.2020.06.007>.

ACKNOWLEDGMENTS

We thank Keller lab members for their advice and comments on the manuscript and experiments. We thank the University Health Network (UHN)/Sick-Kids flow cytometry sorting facility, UHN Pathology Research Program, and Advanced Optical Microscopy Facility at the Princess Margaret Cancer Research Tower for their technical expertise. We also thank Henry Hong and Audrey Chong of the University of Toronto Cell and Systems Biology department imaging facility for their technical expertise with scanning electron microscopy. This work was funded in part by the University of Toronto's Medicine by Design Initiative (G.M.K. and I.D.M.), which receives funding from Canada First Research Excellence Fund (CFREF), and the Canadian Institutes of Health Research (G.M.K., FDN159937). B.K.G. received postdoctoral funding support from the Canadian Institutes of Health Research.

AUTHOR CONTRIBUTIONS

B.K.G. conceived the project, performed experiments, analyzed data, and wrote the manuscript. J.C.L., B.T.I., and G.D.B. analyzed scRNA-seq data and provided valuable input on the manuscript. S.A.M. and I.D.M. harvested the human caudate specimens, isolated primary human LSECs, and provided valuable input on the manuscript. G.M.K. designed the project and wrote the manuscript.

DECLARATION OF INTERESTS

G.M.K. is a founding investigator and a paid consultant for BlueRock Therapeutics LP, a paid consultant for VistaGen Therapeutics, and a member of the board of Anagenesis Biotechnologies. B.K.G. and G.M.K. declare a patent titled "Methods of Producing Venous Angioblasts and Sinusoidal Endothelial Cell – Like Cells and Compositions Thereof" (no. PCT/IB2019/057882) filed September 18, 2019 related to this work.

Received: June 4, 2019
Revised: March 12, 2020
Accepted: June 9, 2020
Published: July 7, 2020

REFERENCES

- Arai, T., Sakurai, T., Kamiyoshi, A., Ichikawa-Shindo, Y., Iinuma, N., Iesato, Y., Koyama, T., Yoshizawa, T., Uetake, R., Yamauchi, A., et al. (2011). Induction of LYVE-1/stabilin-2-positive liver sinusoidal endothelial-like cells from embryoid bodies by modulation of adrenomedullin-RAMP2 signaling. *Peptides* 32, 1855–1865.
- Ben-Moshe, S., and Itzkovitz, S. (2019). Spatial heterogeneity in the mammalian liver. *Nat. Rev. Gastroenterol. Hepatol.* 16, 395–410.
- Blanchette, V.S., Key, N.S., Ljung, L.R., Manco-Johnson, M.J., van den Berg, H.M., and Srivastava, A.; Subcommittee on Factor VIII, Factor IX, and Rare Coagulation Disorders of the Scientific and Standardization Committee of the International Society on Thrombosis and Hemostasis (2014). Definitions in hemophilia: communication from the SSC of the ISTH. *J. Thromb. Haemost.* 12, 1935–1939.
- Braet, F., and Wisse, E. (2002). Structural and functional aspects of liver sinusoidal endothelial cell fenestrae: a review. *Comp. Hepatol.* 1, 1.
- Davidson, K.C., Adams, A.M., Goodson, J.M., McDonald, C.E., Potter, J.C., Berndt, J.D., Biechele, T.L., Taylor, R.J., and Moon, R.T. (2012). Wnt/ β -catenin signaling promotes differentiation, not self-renewal, of human embryonic stem cells and is repressed by Oct4. *Proc. Natl. Acad. Sci. USA* 109, 4485–4490.
- Deleve, L.D. (2013a). Liver sinusoidal endothelial cells and liver injury. In *Drug-Induced Liver Disease*, N. Kaplowitz and L.D. Deleve, eds. (Marcel Dekker), pp. 135–143.
- DeLeve, L.D. (2013b). Liver sinusoidal endothelial cells and liver regeneration. *J. Clin. Invest.* 123, 1861–1866.
- Ding, B.S., Nolan, D.J., Butler, J.M., James, D., Babazadeh, A.O., Rosenwaks, Z., Mittal, V., Kobayashi, H., Shido, K., Lyden, D., et al. (2010). Inductive angiocrine signals from sinusoidal endothelium are required for liver regeneration. *Nature* 468, 310–315.
- Ding, B.S., Cao, Z., Lis, R., Nolan, D.J., Guo, P., Simons, M., Penfold, M.E., Shido, K., Rabbany, S.Y., and Rafii, S. (2014). Divergent angiocrine signals from vascular niche balance liver regeneration and fibrosis. *Nature* 505, 97–102.
- Ditadi, A., Sturgeon, C.M., Tober, J., Awong, G., Kennedy, M., Yzaguirre, A.D., Azzola, L., Ng, E.S., Stanley, E.G., French, D.L., et al. (2015). Human definitive haemogenic endothelium and arterial vascular endothelium represent distinct lineages. *Nat. Cell Biol.* 17, 580–591.
- Elvevold, K.H., Nedredal, G.I., Revhaug, A., and Smedsrød, B. (2004). Scavenger properties of cultivated pig liver endothelial cells. *Comp. Hepatol.* 3, 4.
- Elvevold, K., Simon-Santamaria, J., Hasvold, H., McCourt, P., Smedsrød, B., and Sørensen, K.K. (2008a). Liver sinusoidal endothelial cells depend on mannose receptor-mediated recruitment of lysosomal enzymes for normal degradation capacity. *Hepatology* 48, 2007–2015.
- Elvevold, K., Smedsrød, B., and Martinez, I. (2008b). The liver sinusoidal endothelial cell: a cell type of controversial and confusing identity. *Am. J. Physiol. Gastrointest. Liver Physiol.* 294, G391–G400.
- Filali, E.E., Hiralall, J.K., van Veen, H.A., Stolz, D.B., and Seppen, J. (2013). Human liver endothelial cells, but not macrovascular or microvascular endothelial cells, engraft in the mouse liver. *Cell Transplant.* 22, 1801–1811.
- Fish, J.E., and Wythe, J.D. (2015). The molecular regulation of arteriovenous specification and maintenance. *Dev. Dyn.* 244, 391–409.
- Follenzi, A., Benten, D., Novikoff, P., Faulkner, L., Raut, S., and Gupta, S. (2008). Transplanted endothelial cells repopulate the liver endothelium and correct the phenotype of hemophilia A mice. *J. Clin. Invest.* 118, 935–945.
- Fomin, M.E., Zhou, Y., Beyer, A.I., Publicover, J., Baron, J.L., and Muench, M.O. (2013). Production of factor VIII by human liver sinusoidal endothelial cells transplanted in immunodeficient uPA mice. *PLoS ONE* 8, e77255.
- Fomin, M.E., Beyer, A.I., and Muench, M.O. (2017). Human fetal liver cultures support multiple cell lineages that can engraft immunodeficient mice. *Open Biol.* 7, 170108.
- Ganesan, L.P., Kim, J., Wu, Y., Mohanty, S., Phillips, G.S., Birmingham, D.J., Robinson, J.M., and Anderson, C.L. (2012). Fc γ R1b on liver sinusoidal endothelium clears small immune complexes. *J. Immunol.* 189, 4981–4988.
- Halpern, K.B., Shenhav, R., Matcovitch-Natan, O., Toth, B., Lemze, D., Golan, M., Massasa, E.E., Baydatch, S., Landen, S., Moor, A.E., et al. (2017). Single-cell spatial reconstruction reveals global division of labour in the mammalian liver. *Nature* 542, 352–356.
- Halpern, K.B., Shenhav, R., Massalha, H., Toth, B., Egozi, A., Massasa, E.E., Medgalia, C., David, E., Giladi, A., Moor, A.E., et al. (2018). Paired-cell sequencing enables spatial gene expression mapping of liver endothelial cells. *Nat. Biotechnol.* 36, 962–970.
- Hasan, S.S., Tsaryk, R., Lange, M., Wisniewski, L., Moore, J.C., Lawson, N.D., Wojciechowska, K., Schnittler, H., and Siekmann, A.F. (2017). Endothelial Notch signalling limits angiogenesis via control of artery formation. *Nat. Cell Biol.* 19, 928–940.
- Hen, G., Nicenboim, J., Mayseless, O., Asaf, L., Shin, M., Busolin, G., Hofi, R., Almog, G., Tiso, N., Lawson, N.D., and Yaniv, K. (2015). Venous-derived angioblasts generate organ-specific vessels during zebrafish embryonic development. *Development* 142, 4266–4278.
- Hippenstiel, S., Witzernath, M., Schmeck, B., Hocke, A., Krisp, M., Krüll, M., Seybold, J., Seeger, W., Rascher, W., Schütte, H., and Suttrop, N. (2002). Adrenomedullin reduces endothelial hyperpermeability. *Circ. Res.* 91, 618–625.
- Horn, T., Christoffersen, P., and Henriksen, J.H. (1987). Alcoholic liver injury: defenestration in noncirrhotic livers—a scanning electron microscopic study. *Hepatology* 7, 77–82.
- Hu, J., Srivastava, K., Wieland, M., Runge, A., Mogler, C., Besemfelder, E., Terhardt, D., Vogel, M.J., Cao, L., Korn, C., et al. (2014). Endothelial cell-derived angiopoietin-2 controls liver regeneration as a spatiotemporal rheostat. *Science* 343, 416–419.
- Ichikawa-Shindo, Y., Sakurai, T., Kamiyoshi, A., Kawate, H., Iinuma, N., Yoshizawa, T., Koyama, T., Fukuchi, J., Iimuro, S., Moriyama, N., et al. (2008). The GPCR modulator protein RAMP2 is essential for angiogenesis and vascular integrity. *J. Clin. Invest.* 118, 29–39.
- Innes, B.T., and Bader, G.D. (2018). scClustViz: single-cell RNAseq cluster assessment and visualization. *F1000Res.* 7, J-1522.
- Irion, S., Luche, H., Gadue, P., Fehling, H.J., Kennedy, M., and Keller, G. (2007). Identification and targeting of the ROSA26 locus in human embryonic stem cells. *Nat. Biotechnol.* 25, 1477–1482.
- Korsunsky, I., Millard, N., Fan, J., Slowikowski, K., Zhang, F., Wei, K., Baglaenko, Y., Brenner, M., Loh, P.R., and Raychaudhuri, S. (2019). Fast, sensitive and accurate integration of single-cell data with Harmony. *Nat. Methods* 16, 1289–1296.
- Koui, Y., Kido, T., Ito, T., Oyama, H., Chen, S.W., Katou, Y., Shirahige, K., and Miyajima, A. (2017). An in vitro human liver model by iPSC-derived parenchymal and non-parenchymal cells. *Stem Cell Reports* 9, 490–498.
- Koyama, T., Ochoa-Callejero, L., Sakurai, T., Kamiyoshi, A., Ichikawa-Shindo, Y., Iinuma, N., Arai, T., Yoshizawa, T., Iesato, Y., Lei, Y., et al. (2013). Vascular endothelial adrenomedullin-RAMP2 system is essential for vascular integrity and organ homeostasis. *Circulation* 127, 842–853.
- MacParland, S.A., Liu, J.C., Ma, X.Z., Innes, B.T., Bartczak, A.M., Gage, B.K., Manuel, J., Khuu, N., Echeverri, J., Linares, I., et al. (2018). Single cell RNA sequencing of human liver reveals distinct intrahepatic macrophage populations. *Nat. Commun.* 9, 4383.
- Martinez, I., Nedredal, G.I., Øie, C.I., Warren, A., Johansen, O., Le Couteur, D.G., and Smedsrød, B. (2008). The influence of oxygen tension on the structure and function of isolated liver sinusoidal endothelial cells. *Comp. Hepatol.* 7, 4.
- Mousavi, S.A., Sporstøl, M., Fladeby, C., Kjekken, R., Barois, N., and Berg, T. (2007). Receptor-mediated endocytosis of immune complexes in rat liver sinusoidal endothelial cells is mediated by Fc γ R1b2. *Hepatology* 46, 871–884.

- Nonaka, H., Tanaka, M., Suzuki, K., and Miyajima, A. (2007). Development of murine hepatic sinusoidal endothelial cells characterized by the expression of hyaluronan receptors. *Dev. Dyn.* 236, 2258–2267.
- Nonaka, H., Watabe, T., Saito, S., Miyazono, K., and Miyajima, A. (2008). Development of stabilin2+ endothelial cells from mouse embryonic stem cells by inhibition of TGFβ/activin signaling. *Biochem. Biophys. Res. Commun.* 375, 256–260.
- Olgasi, C., Talmon, M., Merlin, S., Cucci, A., Richaud-Patin, Y., Ranaldo, G., Colangelo, D., Di Scipio, F., Berta, G.N., Borsotti, C., et al. (2018). Patient-specific iPSC-derived endothelial cells provide long-term phenotypic correction of hemophilia A. *Stem Cell Reports* 11, 1391–1406.
- Prasain, N., Lee, M.R., Vemula, S., Meador, J.L., Yoshimoto, M., Ferkowicz, M.J., Fett, A., Gupta, M., Rapp, B.M., Saadatzadeh, M.R., et al. (2014). Differentiation of human pluripotent stem cells to cells similar to cord-blood endothelial colony-forming cells. *Nat. Biotechnol.* 32, 1151–1157.
- Reubinoff, B.E., Pera, M.F., Fong, C.Y., Trounson, A., and Bongso, A. (2000). Embryonic stem cell lines from human blastocysts: somatic differentiation in vitro. *Nat. Biotechnol.* 18, 399–404.
- Schindelin, J., Arganda-Carreras, I., Frise, E., Kaynig, V., Longair, M., Pietzsch, T., Preibisch, S., Rueden, C., Saalfeld, S., Schmid, B., et al. (2012). Fiji: an open-source platform for biological-image analysis. *Nat. Methods* 9, 676–682.
- Shahani, T., Covens, K., Lavend'homme, R., Jazouli, N., Sokal, E., Peerlinck, K., and Jacquemin, M. (2014). Human liver sinusoidal endothelial cells but not hepatocytes contain factor VIII. *J. Thromb. Haemost.* 12, 36–42.
- Shindo, T., Kurihara, Y., Nishimatsu, H., Moriyama, N., Kakoki, M., Wang, Y., Imai, Y., Ebihara, A., Kuwaki, T., Ju, K.H., et al. (2001). Vascular abnormalities and elevated blood pressure in mice lacking adrenomedullin gene. *Circulation* 104, 1964–1971.
- Sriram, G., Tan, J.Y., Islam, I., Rufaihah, A.J., and Cao, T. (2015). Efficient differentiation of human embryonic stem cells to arterial and venous endothelial cells under feeder- and serum-free conditions. *Stem Cell Res. Ther.* 6, 261.
- Srivastava, A., Brewer, A.K., Mauser-Bunschoten, E.P., Key, N.S., Kitchen, S., Linas, A., Ludlam, C.A., Mahlangu, J.N., Mulder, K., Poon, M.C., and Street, A.; Treatment Guidelines Working Group on Behalf of The World Federation Of Hemophilia (2013). Guidelines for the management of hemophilia. *Haemophilia* 19, e1–e47.
- Stewart, M.H., Bossé, M., Chadwick, K., Menendez, P., Bendall, S.C., and Bhatia, M. (2006). Clonal isolation of hESCs reveals heterogeneity within the pluripotent stem cell compartment. *Nat. Methods* 3, 807–815.
- Strauss, O., Phillips, A., Ruggiero, K., Bartlett, A., and Dunbar, P.R. (2017). Immunofluorescence identifies distinct subsets of endothelial cells in the human liver. *Sci. Rep.* 7, 44356.
- Sturgeon, C.M., Ditadi, A., Awong, G., Kennedy, M., and Keller, G. (2014). Wnt signaling controls the specification of definitive and primitive hematopoiesis from human pluripotent stem cells. *Nat. Biotechnol.* 32, 554–561.
- White, G.C., 2nd, Rosendaal, F., Aledort, L.M., Lusher, J.M., Rothschild, C., and Ingerslev, J.; Factor VIII and Factor IX Subcommittee (2001). Definitions in hemophilia. Recommendation of the scientific subcommittee on factor VIII and factor IX of the scientific and standardization committee of the International Society on Thrombosis and Haemostasis. *Thromb. Haemost.* 85, 560.
- Wisse, E., De Zanger, R.B., Charels, K., Van Der Smissen, P., and McCuskey, R.S. (1985). The liver sieve: considerations concerning the structure and function of endothelial fenestrae, the sinusoidal wall and the space of Disse. *Hepatology* 5, 683–692.
- Xie, G., Wang, L., Wang, X., Wang, L., and DeLeve, L.D. (2010). Isolation of periportal, midlobular, and centrilobular rat liver sinusoidal endothelial cells enables study of zonated drug toxicity. *Am. J. Physiol. Gastrointest. Liver Physiol.* 299, G1204–G1210.
- Zhang, H., Pu, W., Tian, X., Huang, X., He, L., Liu, Q., Li, Y., Zhang, L., He, L., Liu, K., et al. (2016). Genetic lineage tracing identifies endocardial origin of liver vasculature. *Nat. Genet.* 48, 537–543.
- Zhang, J., Chu, L.F., Hou, Z., Schwartz, M.P., Hacker, T., Vickerman, V., Swanson, S., Leng, N., Nguyen, B.K., Elwell, A., et al. (2017). Functional characterization of human pluripotent stem cell-derived arterial endothelial cells. *Proc. Natl. Acad. Sci. USA* 114, E6072–E6078.
- Zhong, T.P., Childs, S., Leu, J.P., and Fishman, M.C. (2001). Gridlock signaling pathway fashions the first embryonic artery. *Nature* 414, 216–220.

STAR★METHODS

KEY RESOURCES TABLE

REAGENT or RESOURCE	SOURCE	IDENTIFIER
Antibodies		
Mouse monoclonal to CD34-PECy7 (clone 4H11)	EBiosciences	Cat# 25-0349-42; RRID: AB_1963576
Mouse monoclonal to CD34-APC (clone 8G12)	BD Biosciences	Cat# 340441; RRID: AB_400514
Mouse monoclonal to CD31-PE (clone WM59)	BD Biosciences	Cat# 555446; RRID: AB_395839
Mouse monoclonal to CD31-FITC (clone WM59)	BD Biosciences	Cat# 555445; RRID: AB_395838
Mouse monoclonal to CD31-AF647 (clone WM59)	BD Biosciences	Cat# 561654; RRID: AB_10896969
Mouse monoclonal to CD31-APCCy7 (clone WM59)	BD Biosciences	Cat# 563653; RRID: AB_2738350
Mouse monoclonal to CD184-BV421 (clone 12G5)	BioLegend	Cat# 306518; RRID: AB_11146018
Mouse monoclonal to CD73-APC (clone AD2)	BD Biosciences	Cat# 560847; RRID: AB_10612019
Mouse monoclonal to CD32-PE (clone FUN-2)	BioLegend	Cat# 303206; RRID: AB_314338
Mouse monoclonal to CD32-PECy7 (clone FUN-2)	BioLegend	Cat# 303214; RRID: AB_2616923
Mouse monoclonal to KDR-biotin (clone 89106), custom biotinylated	R&D Systems	Cat# MAB3572; RRID: AB_2132190
Mouse monoclonal to CD56-APC (clone B159)	BD Biosciences	Cat# 555518; RRID: AB_398601
Mouse monoclonal to CD235a/b-APC (clone GA-R2/HIR2)	BD Biosciences	Cat# 551336; RRID: AB_398499
Mouse monoclonal to CD140b (PDGFR β)-BV421 (clone 28D4)	BD Horizon	Cat# 564124; RRID: AB_2738609
Mouse monoclonal to CD45-PECy5.5 (clone HI30)	BioLegend	Cat# 304010; RRID: AB_314398
Mouse monoclonal to CD68-AF488 (clone Y1.82A)	BioLegend	Cat# 333812; RRID: AB_2074832
Rabbit polyclonal to LYVE1	Abcam	Cat# ab36993; RRID: AB_2138663
Rabbit polyclonal to NFAT2/NFATC1	Abcam	Cat# ab25916; RRID: AB_448901
Rabbit polyclonal to GATA4	Abcam	Cat# ab84593; RRID: AB_10670538
Mouse monoclonal anti human CD31 (clone JC70A)	DAKO	Cat# M0823; RRID: AB_2114471
Rabbit polyclonal anti HEY2	Proteintech	Cat# 10597-1-AP; RRID: AB_2118415
Mouse monoclonal anti COUPTFII (clone H7147)	R&D Systems	Cat# PP-H7147-00; RRID: AB_2155627
Goat polyclonal anti VE-CAD	SantaCruz	Cat# SC-6458; RRID: AB_207795
Goat polyclonal anti human CD32B	NSJ Bioreagents	Cat# R34966; RRID: AB_2833066
Sheep polyclonal anti human Stabilin2	R&D Systems	Cat# AF3645; RRID: AB_2194929
Mouse monoclonal anti MRC1 (clone 685645)	R&D Systems	Cat# MAB25341; RRID: AB_10890782
Rabbit monoclonal anti human Ku80 (clone C48E7)	Cell Signaling	Cat# 2180; RRID: AB_2218736

(Continued on next page)

Continued

REAGENT or RESOURCE	SOURCE	IDENTIFIER
Mouse monoclonal anti human FVIII (clone 27.4)	Abcam	Cat# ab41188; RRID: AB_732287
Rat monoclonal anti mouse F4/80 (clone Cl:A3-1)	Bio-Rad	Cat# MCA497GA; RRID: AB_323806
Rabbit monoclonal anti human SMA (clone E184)	Abcam	Cat# ab32575; RRID: AB_722538
Mouse monoclonal anti human Vimentin (clone V9)	Sigma-Aldrich	Cat# V6630; RRID: AB_477627
Rabbit polyclonal anti Collagen I	Abcam	Cat# ab34710; RRID: AB_731684
Rabbit polyclonal anti Collagen III	Abcam	Cat# ab7778; RRID: AB_306066
Donkey anti-rabbit IgG-APC, F(ab') ₂	Jackson	Cat# 711-136-152; RRID: AB_2340601
Donkey anti-mouse IgG-AF488 (H+L)	ThermoFisher	Cat# A-21202; RRID: AB_141607
Donkey anti-mouse IgG-AF555 (H+L)	ThermoFisher	Cat# A-31570; RRID: AB_2536180
Donkey anti-mouse IgG-AF647 (H+L)	ThermoFisher	Cat# A-31571; RRID: AB_162542
Donkey anti-rabbit IgG-AF488 (H+L)	ThermoFisher	Cat# A-21206; RRID: AB_2535792
Donkey anti-rabbit IgG-AF555 (H+L)	ThermoFisher	Cat# A-31572; RRID: AB_162543
Donkey anti-rabbit IgG-AF647 (H+L)	ThermoFisher	Cat# A-31573; RRID: AB_2536183
Donkey anti-goat IgG-AF488 (H+L)	ThermoFisher	Cat# A-11055; RRID: AB_2534102
Donkey anti-goat IgG-AF555 (H+L)	ThermoFisher	Cat# A-21432; RRID: AB_2535853
Donkey anti-goat IgG-AF647 (H+L)	ThermoFisher	Cat# A-21447; RRID: AB_2535864
Donkey anti-sheep IgG-AF488 (H+L)	ThermoFisher	Cat# A-11015; RRID: AB_2534082
Donkey anti-rat IgG-AF488 (H+L)	ThermoFisher	Cat# A-21208; RRID: AB_2535794
Streptavidin-PECy7	BD Biosciences	Cat# 557598
Streptavidin-BV421	BioLegend	Cat# 405225
Biological Samples		
HUVEC	Lonza	Cat# C125AS
Dissociated Primary Human Liver Tissue	MacParland et al., 2018 ; This study	N/A
Chemicals, Peptides, and Recombinant Proteins		
DAPI	Biotium	Cat# 40043
FcR Blocking Reagent (human IgG)	Miltenyi Biotec	Cat# 130-059-901
Ammonium Chloride	STEMCELL Technologies	Cat# 07850
Monocrotaline	Sigma-Aldrich	Cat# C2401
Penicillin/streptomycin	ThermoFisher	Cat# 15070063
L-glutamine	ThermoFisher	Cat# 25030081
Non-essential amino acids	ThermoFisher	Cat# 11140-050
Transferrin	ROCHE	Cat# 10652202001
Ascorbic acid	Sigma-Aldrich	Cat# A4544
Monothioglycerol	Sigma-Aldrich	Cat# M-6145
β-Mercaptoethanol	ThermoFisher	Cat# 21985-023
ROCK inhibitor Y-27632	Tocris	Cat# 1254
Recombinant human BMP4	R&D Systems	Cat# 314-BP
Recombinant human bFGF	R&D Systems	Cat# 233-FB
Recombinant human VEGF-A	R&D Systems	Cat# 293-VE
Recombinant human VEGF-C	R&D Systems	Cat# 9199-VC
CHIR 99021 (GSK-3 inhibitor)	Tocris	Cat# 4423
L-685-458 (Notch inhibitor, GSI)	Tocris	Cat# 2627
SB-431542 (TGFβ inhibitor, SB)	Sigma-Aldrich	Cat# S4317
8-Br-cAMP (cAMP)	Biolog	Cat# B 007
IOX2	Sigma-Aldrich	Cat# SML0652

(Continued on next page)

REAGENT or RESOURCE	SOURCE	IDENTIFIER
Continued		
Critical Commercial Assays		
VisuLize Factor VIII Antigen Kit (Lot:AG8-0050)	Affinity Biologicals	Cat# FVIII-AG
Formaldehyde-treated serum albumin, FITC labeled	D'Liver	Cat# FSA-F
Acetylated LDL-AF488	Invitrogen	Cat# L23380
E.coli BioParticles-AF594	Invitrogen	Cat# E23370
Human CD34 MicroBead Isolation kit	Miltenyi Biotec	Cat# 130-046-702
Human CD31 MicroBead Isolation kit	Miltenyi Biotec	Cat# 130-091-935
MS columns	Miltenyi Biotec	Cat# 130-042-201
LS columns	Miltenyi Biotec	Cat# 130-042-401
RNAqueous-micro kit with RNase-free DNase treatment	Ambion	Cat# AM1931
iSCRIPT	Bio-Rad	Cat# 1798841
QuantiFast SYBR Green PCR mix	QIAGEN	Cat# 204057
Histological Mouse and Rabbit Detection kit – MACH4	Inter Medico	Cat# BC-M4U534L
Histological Rabbit Detection kit – IMPRESS-AP	Vector	Cat# MP5401-15
Histological Developer kit, Warp Red	Inter Medico	Cat# BC-WR806H
Histological Developer kit, DAB	DAKO	Cat# K3468
10x Genomics Single-Cell 3' V2 Reagents	10x Genomics	Single Cell 3' v2
Deposited Data		
Primary Human Liver scRNaseq	MacParland et al., 2018	GEO: GSE115469
hPSC-Venous Angioblast-derived <i>in vivo</i> matured LSECs - scRNaseq	This study	GEO: GSE131987
Experimental Models: Cell Lines		
Human ESC: HES2	Reubinoff et al., 2000	RRID: CVCL_D093
Human ESC: HES2:tdRFP	Irion et al., 2007	N/A
Human ESC: HES2:eGFP	Irion et al., 2007	N/A
Human ESC: H1-eGFP	Davidson et al., 2012	N/A
Experimental Models: Organisms/Strains		
NSG mice: NOD.Cg Prkdcscidll2rgtm1Wjl/SzJ	The Jackson Laboratory; OCI colony	Cat# 005557
Oligonucleotides		
Primers for RT-qPCR	This study	Table S4
Software and Algorithms		
FlowJo	Tree Star; https://www.flowjo.com	Version 10
GraphPad Prism	GraphPad Software; https://www.graphpad.com/scientific-software/prism	Version 8
ImageJ (FIJI)	FIJI (Schindelin et al., 2012); https://imagej.nih.gov/ij/	Version 2.0.0-rc-69/1.52p
Aperio Image Scope	Leica Biosystems; https://www.leicabiosystems.com/digital-pathology/manage/aperio-imagescope/	Version 12.4.3
R CRAN	https://cran.r-project.org/	Version 3.5
Cell Ranger	https://support.10xgenomics.com/single-cell-gene-expression/software/pipelines/latest/what-is-cell-ranger	10x Genomics, version 2.1.0
Scran	https://git.bioconductor.org/packages/scran	Version 1.12.1

(Continued on next page)

Continued

REAGENT or RESOURCE	SOURCE	IDENTIFIER
Seurat	https://github.com/satijalab/seurat	Version 2.3.0
Harmony Integration	Korsunsky et al., 2019; https://github.com/immunogenomics/harmony	N/A
Pearson Correlation R base	https://cran.r-project.org/	N/A
Other		
Universal protein blocking solution	Agilent (DAKO)	Cat# X090930-2
Universal antibody diluent	Agilent (DAKO)	Cat# S080983-2
ProLong diamond antifade mounting medium	ThermoFisher	Cat# P36965
PBS -Mg -Ca	GIBCO	Cat# 14190-250
PBS +Mg +Ca	GIBCO	Cat# 14040-182
StemPro-34 media	ThermoFisher	Cat# 10639011
DMEM/F12	Cellgro	Cat# 10-092-CV
KnockOut serum replacement	ThermoFisher	Cat# 10828028
TrypLE	ThermoFisher	Cat# 12605010
Trypsin/EDTA	Corning	Cat# 25-053-CI
Collagenase Type 1	Sigma-Aldrich	Cat# C0130
IMDM	GIBCO	Cat# 12200069
DNase I	Millipore	Cat# 260913
RPMI 1640	GIBCO	Cat# 11875-093
EBM-2 (Endothelial Basal Medium)	Lonza	Cat# CC-3156
EGM-2 (SingleQuots supplement kit for EBM-2)	Lonza	Cat# CC-4176
Cryostore CS10	STEMCELL Technologies	Cat# 07930
Saline – 100ml bag	Baxter	Cat# JB1306
Hanks Buffered Salt Solution	GIBCO	Cat# 14175-079
Cell Culture Grade Water	Corning	Cat# 25-055-CM
Fetal calf serum	Wisent	Cat# 080-150
Bovine serum albumin	Sigma-Aldrich	Cat# A1470
Matrigel, growth factor reduced (GFR)	Corning	Cat# 356230

RESOURCE AVAILABILITY

Lead Contact

Further information and requests for resources and reagents should be directed to and will be fulfilled by the Lead Contact, Dr. Gordon Keller (Gordon.keller@uhnresearch.ca).

Materials Availability

This study did not generate unique reagents.

Data and Code Availability

The accession number for the scRNA-seq dataset reported in this paper is GEO: GSE131987. All other datasets and code are available upon request from the Lead Contact or directly from the lab of Dr. Gary D. Bader. Analyzed data are also available for interactive viewing through scClustViz at <http://shiny.baderlab.org/hPSCLECsAndHumanLiver/>.

EXPERIMENTAL MODEL AND SUBJECT DETAILS

Animals

All experiments were done in accordance with institutional guidelines approved by the University Health Network Animal care committee. NSG mice (NOD.Cg PrkdcscidIl2rgtm1Wjl /SzJ; Jackson Laboratory, local Ontario Cancer Institute colony) were utilized as 6-10 week old adults (both sexes) or from timed mating's to generate neonatal NSG pups (both sexes) for transplantation tests. Animals were maintained under standard conditions (12-hour light/dark cycle) on ventilated racks equipped with sterile micro-isolation

caging (up to 5 mice per cage) in a specific-pathogen free facility (UHN, Toronto, ON). Mice were housed on corn-cob bedding with environmental enrichment, cotton nestlet, and *ad libitum* access to standard irradiated diet (Harland-Teklad LM-485 7912). Pregnant females were provided with 11% fat diet from ~E12.5 to weaning.

Cell Lines

HES2 hESCs (Reubinoff et al., 2000) (karyotype: 46, XX) were previously targeted at the human ROSA locus to enable constitutive tdRFP or eGFP expression (Irion et al., 2007). H1-GFP hESCs (karyotype: 46, XY) were a gift by R. Moon (University of Washington, Seattle, USA) and were generated from H1 hESCs by lentiviral transduction of pMIN-Ub-GFP-WPRE (Stewart et al., 2006) (Davidson et al., 2012). hPSC lines were maintained on gelatin coated dishes with irradiated mouse embryonic fibroblasts in hPSC culture media consisting of DMEM/F12 (Cellgro) supplemented with penicillin/streptomycin (1%, ThermoFisher), L-glutamine (2mM, ThermoFisher), non-essential amino acids (1x, ThermoFisher), β -mercaptoethanol (55 μ M, ThermoFisher), KnockOut serum replacement (20% v/v, ThermoFisher) and rhbFGF (10-20ng/ml optimized for each line, R&D). Cell lines were confirmed to be karyotypically normal and free from detectable mycoplasma within two passages of experimental use. Cell lines were authenticated by providence, karyotype, and confirmation of expected fluorescent protein expression patterns.

Primary Cell Cultures

HUVECs

Human Umbilical Vein Endothelial Cells (HUVECs) were purchased as a multi-donor, unknown-sex, pool from Lonza (Cat#C125AS) and maintained in EGM2 medium (LONZA) on Matrigel coated tissue culture plates. Cells were used between passage 3-4 of arrival for both *in vitro* and *in vivo* work.

Human Liver Tissue

Human liver tissue was obtained from livers procured from deceased donors deemed acceptable for liver transplantation. At the University Health Network (UHN), the caudate lobe (segment 1) of the liver is often removed in preparation of the organ for implantation. Previously reported samples were collected with appropriate institutional ethics approval from the UHN (REB# 14-7425-AE) and processed as described previously (MacParland et al., 2018). During organ retrieval, donor liver grafts were perfused *in situ* with cold (HTK) solution (Methapharm) to thoroughly flush circulating cells, leaving only tissue resident cells in the caudate that were then used to prepare single-cell suspensions for scRNA-seq or flow cytometric analysis. The removed caudate lobe was then dissociated using the protocol as fully described (<https://www.protocols.io/view/human-liver-caudate-lobe-dissociation-for-scRNA-seq-m9sc96e>) and use in flow cytometric LSEC isolation detailed below.

METHOD DETAILS

Directed Differentiation of Angioblasts from hESCs

hESC differentiation was performed in embryoid bodies (EBs) adapted from our previous hemato-vascular strategy (Sturgeon et al., 2014). Except where noted, all differentiation experiments were under hypoxic conditions (5% CO₂, 5% O₂, 90% N₂). At day -1, 85%–95% confluent hESCs were dissociated to single cells (3-4 mins, TrypLE, ThermoFisher) and re-aggregated to form EBs at a cell density optimized for each line (generally 5x10⁵ cells/ml) to achieve uniform ~75 μ m diameter EBs after 18 hours of orbital rotation shaking at 60RPM (MaxQ 2000 shaker, ThermoFisher). Re-aggregation was carried out in “base media” consisting of StemPro34 (25%v/v, ThermoFisher), IMDM (75%v/v, ThermoFisher), ITS-X (1:10,000, ThermoFisher), penicillin/streptomycin (1%, ThermoFisher), L-glutamine (2mM, ThermoFisher), ascorbic acid (50 μ g/ml, Sigma-Aldrich), transferrin (150 μ g/ml, ROCHE), and monothio-glycerol (50 μ g/ml, Sigma-Aldrich), supplemented for re-aggregation with ROCK inhibitor (Y-27623, 10 μ M, TOCRIS) and rhBMP4 (1ng/ml, R&D). As indicated in Figure 1A, at day 0, the aggregates were transferred to base media that contained higher concentrations of rhBMP4 (10ng/ml) but no ROCK inhibitor in 6-well or 10cm tissue culture plates (Corning) that were coated with PolyHema (5%w/v in 95% ethanol, Sigma-Aldrich, dried overnight) to prevent cell adhesion. At day 1, EBs were refed with base media supplemented with rhBMP4 (10ng/ml) and rhbFGF (5ng/ml final concentration). At day 2, EBs were separated from single cell debris and transferred to definitive hematopoietic mesoderm media that consists of base media supplemented with rhBMP4 (10ng/ml), rhbFGF (5ng/ml), CHIR99021 (3 μ M, TOCRIS). Day 4 EBs were transferred to angioblast induction conditions made up of base media supplemented with either arterial: rhbFGF (30ng/ml) and rhVEGF-A (100ng/ml, R&D) or venous: rhbFGF (30ng/ml), rhVEGF-A (10ng/ml), and GSI (L-685-458, 10 μ M, TOCRIS) inducing factors. Day 6 EBs were cleaned of debris by differential centrifugation and replated in angioblast induction conditions. On day 8, the EBs were dissociated by sequential addition of trypsin EDTA (5 mins, 37°C, Corning), stopped with 50%v/v fetal calf serum (FCS, Wiscent)/IMDM, Collagenase Type 1 (0.2%w/v, 60 mins, 37°C, Sigma-Aldrich, in 20% FCS) followed by light trituration. Single cell suspensions were enriched for CD34⁺ angioblasts by magnetic activated cell sorting (MACS, Miltenyi, 130-146-702) using 10 μ l antibody / 5x10⁶ cells/100 μ l in base media supplemented with DNASE (1U/ml, Millipore) for 30 minutes at 4°C. Angioblasts were purified by two columns in series (either MS or LS depending on cell number) to isolate populations consisting of 95% CD34⁺ cells or greater for future experiments. After purification, CD34⁺ cells were used immediately in downstream applications or cryopreserved (1-1.5x10⁶ cells/0.5ml Cryostore CS10, STEMCELL Technologies).

To generate endothelial cells and later LSEC-LCs, fresh or frozen day 8 angioblasts were plated (2.6 × 10⁴ cells / cm²) on diluted GFR-Matrigel coated (2.5%v/v in IMDM, 30 minutes - 7 days at 4°C, 1-4 hours at 37°C, Corning) tissue culture plates in base media supplemented with ROCK inhibitor (10 μ M) with either arterial EC: rhbFGF (30ng/ml) and rhVEGF-A (100ng/ml) or venous EC: rhbFGF

(30ng/ml), rhVEGF-A (10ng/ml) supplements. On day 9, media was replaced with day 8 medias without ROCK inhibitor. On day 11, cultures (generally 60% confluent) were top fed half volume with respective arterial or venous EC medias such that by day 12 cultures had just reached confluency. From days 12-22, endothelial expansion media was removed and replaced every two days with fresh LSEC-LC marker induction media comprised of base media supplemented with rhbFGF (30ng/ml), 8-Br-cAMP (cAMP, 1mM, Biolog) and TGF- β inhibitor SB-431542 (SB, 6 μ M, Sigma-Aldrich).

Angioblast Specification and LSEC Marker Induction

Arterial and venous angioblast specification was optimized by treating day 4 EBs with different concentrations of rhVEGF-A (0, 10, 30, 100ng/ml), rhbFGF (0, 10, 30, 100ng/ml), and GSI (0, 3, 10, 30 μ M) in base media. Treatment was followed by trypsin/EDTA mediated dissociation at day 6, the EBs were harvested, the cells counted and analyzed by flow cytometry for expression of CD34, CD31, CD184, CD73 to quantify the proportion of arterial (CD34⁺, CD184⁺, CD73^{+/-}) and venous (CD34⁺, CD184⁻, CD73⁺) angioblasts.

LSEC marker induction was optimized by treating either confluent arterial or venous endothelial cells with different concentrations of cAMP (0, 0.1, 0.3, 1.0 mM), SB (0, 6, 18 μ M) and VEGF-C (0, 100ng/ml, R&D) in base media supplemented with rhbFGF (30ng/ml). Treatment was followed by bulk population RT-qPCR analysis for LSEC markers. Optimized LSEC-LC culture conditions of rhbFGF (30ng/ml), cAMP (1mM), SB (6 μ M) were also used for FACS mediated LSEC marker analysis.

The effect of oxygen tension on LSEC marker expression was assessed by plating angioblasts at day 8 in normoxic (5%CO₂, 95% Air) or hypoxic (5%CO₂, 5%O₂, 90% N₂) culture conditions until analysis (days 12-22). Chemical modulation of HIF1 α signaling was achieved by administration of IOX2 (0, 10, 30, 100, 300 μ M, Sigma-Aldrich) to day 12 arterial or venous endothelial cells along with the LSEC-LC stimuli (base media, 30ng/ml rhbFGF, 1mM cAMP, 6 μ M SB) under controlled oxygen conditions. Flow cytometry or RT-qPCR analysis was performed 4 days later having received IOX2 treatments on day 12 and 14.

Flow Cytometry and FACS

Monolayer cells and day 4 EBs were dissociated with TrypLE for 5-7 minutes at 37°C. Day 6 EBs were dissociated with Trypsin/EDTA for 5 minutes at 37°C. Day 8 EBs were partially dissociated with Trypsin/EDTA for 5 minutes followed by full dissociation with Collagenase type 1 (0.2% w/v in 20% FCS) for 60 minutes at 37°C. The following primary antibodies were used for flow cytometric staining: anti-KDR-biotin (R&D, Clone 89106, 15:100), anti-CD56-APC (BD Biosciences, Clone B159, 5:100), anti-CD235a/b-APC (BD Biosciences, Clone GA-R2/HIR2, 2:100), anti-CD34-PeCy7 (EBiosciences, Clone 4H11, 1:100), anti-CD31-FITC (BD Biosciences, Clone WM59, 15:100), anti-CD31-PE (BD Biosciences, Clone WM59, 5:100), anti-CD31-APCCy7 (BD Biosciences, Clone WM59, 1:100) anti-CD184-BV421 (BioLegend, Clone 12G5, 1:100), anti-CD73-APC (BD Biosciences, Clone AD2, 0.25:100), rabbit-anti-LYVE1 (Abcam, Polyclonal, 1:1000), and anti-CD32-PeCy7 (BioLegend, Clone FUN-2, 3:100), anti-CD140b-BV421 (BD Biosciences, Clone 28D4, 5:100). For unconjugated antibodies, the following secondary systems were used for detection: Streptavidin-PeCy7 (BD Biosciences, 0.5:100), Streptavidin-BV421 (BioLegend, 1:100), Donkey-anti-rabbit-APC (F(ab)₂ fragment, Jackson, 0.5:100).

For *in vitro* surface marker analysis, cells were stained for 30 minutes at 4°C in FACS buffer (PBS without Mg/Ca with 5% FCS (Wisent), 0.02% NaN₃ (Sigma-Aldrich), DNASE (1U/ml)). Prior to staining of cells isolated from dissociated liver tissue, the cells (1x10⁶ cells/100 μ l) were treated with FcR blocking human IgG (Miltenyi, 15:100) in RPMI1640 with 0.5% BSA and 1U/ml DNase along with primary antibodies. Stained cells were analyzed using a LSRII flow cytometer (BD) or a Fortessa flow cytometer equipped with a 532nm green laser (BD). For cell sorting, cells from culture were stained in IMDM with 0.5% FCS, DNASE (0.1U/ml), and DAPI (Biotium, 0.1 μ g/ml). The stained cells were sorted with FACSAriaII (BD) and FACSAriaIII (BD) cell sorters at the Sickkids/UHN flow cytometry facility. Data were analyzed using FlowJo software (version 10.6.1, Tree star).

Primary human LSECs were isolated via a two-step collagenase and neutral protease perfusion/dissociation of multiple (n = 5) surgically resected healthy caudate liver lobes (MacParland et al., 2018). Total liver homogenate samples were depleted of hepatocytes by centrifugation (50xg, 5 minutes) giving a non-parenchymal cell (NPC) fraction that was used for positive cell isolation. Primary LSECs (Live/Dead⁻, CD45⁻, CD68⁻, CD32⁺) were isolated by hematopoietic and macrophage depletion. Briefly, the cells were stained with Live/Dead NIR (BioLegend, 1:100) to assess viable cells and fluorophore-conjugated monoclonal antibodies to the following human cell-surface markers: anti-CD45-PeCy5.5 (BioLegend, Clone: HI30, 1:20), anti-CD68-AF488 (BioLegend, Clone: Y1.82A, 1:20) and anti-CD32-PE (BioLegend, Clone: FUN2, 1:20). Human LSECs were sorted based on CD32 expression on a FACSAriaII (BD) cell sorter following the scheme outlined in supplemental figure S4. Following sorting, the LSECs were immediately frozen along with the total liver homogenate and the unsorted non-parenchymal cell fractions for future RT-qPCR analysis.

Quantitative Reverse Transcription PCR

Total RNA from bulk, MACS-enriched, or FACS-enriched hPSC-derived populations from *in vitro* and *in vivo* sources were isolated using RNAqueous-micro kit with post column DNase treatment. Up to 1 μ g of RNA was reverse transcribed into cDNA using iSCRIPT (BioRad) and RT-qPCR was performed on an EP Real-Plex MasterCycler (Eppendorf) or CFX384 Touch Real-Time instrument (BioRad) using QuantiFast SYBR Green PCR kit (QIAGEN) and primers described in Table S4. All data were generated as technical duplicates evaluated for relative copy number, reaction efficiency, and genomic DNA contamination (< 0.01% of *TBP* content) using a 10-fold dilution series of sonicated human genomic DNA standards made in house from wild-type HES2 hESC cells ranging from 25ng/ μ l to 2.5pg/ μ l. Samples free of genomic DNA contamination were assessed for expression of genes of interest relative to the house keeping gene *TBP*. Heatmaps of gene expression were generated in Prism version 8 (Graphpad).

Neonatal Intrahepatic Transplantation

For neonatal engraftment, P1-P4 NSG pups (bred at the Ontario Cancer Institute colony from timed matings) were irradiated (100 cGy, 18–24 hours before transplant), and injected intrahepatically (30G1/2 needle on a Hamilton syringe) with $1\text{--}1.5 \times 10^6$ cells in 20–30 μl of base media. Cell-dose-matched Day 8 arterial or venous angioblasts (> 95% CD34⁺) or day 14–16 arterial or venous LSEC-LC (> 95% CD31⁺) were injected as either fresh (1×10^6 cells) and/or frozen (1.5×10^6 cells) cell populations in multiple ($n \geq 10$) independent transplantation cohorts. Post thaw viability of the different cell populations was approximately 60%–75% based on DAPI exclusion. After irradiation, mice were transitioned to prophylactic enrofloxacin (Baytril) in the drinking water for the duration of the experiment (up to 125 days post-transplant).

Adult Intrasplenic Transplantation

For adult transplantations, we first optimized monocrotaline conditioning to sublethally induce hepatic endothelial damage. Intraperitoneal injection of monocrotaline (MCT, SIGMA-ALDRICH, 5mg/ml in saline) at increasing doses from 0mg/kg to 300mg/kg was tested for acute toxicity and formation of ascites associated with liver damage over 14 days. No MCT (0/4), 100mg/kg MCT (0/3), 150mg/kg MCT (0/4) doses showed no acute toxicity or ascites, whereas 300mg/kg MCT (5/5) was acutely toxic within 48 hours to all tested mice. Thus, adult NSG mice (6–10 week old male or females) were treated with 150mg/kg MCT 24 hours before cell delivery. Isoflurane anesthetized mice received Tramadol and bupivacaine for pain management associated with laparotomy and intrasplenic injection of 1.5×10^6 frozen day 8 arterial or venous angioblast cells in 50 μl of base media. After cell infusion over 15 s, local cauterization was applied to the splenic surface to control bleeding. After surgery, mice were transitioned to enrofloxacin for the remainder of the experiment.

Non-Parenchymal Cell Isolation and *ex vivo* Analysis

At various time points after transplantation (day 30–125), NSG mice were sacrificed to enable histological assessment and liver dissociation for RFP⁺ cell recovery by FACS. To provide a matched plasma sample and recover engrafted cells from liver tissue, freshly euthanized mice underwent cardiac blood sampling followed by aseptic *in situ* perfusion of 3–5ml of type 1 collagenase (0.2% w/v in 20% FCS/PBS) via a 26G1/2 needle cannulated portal vein. Perfused, dissected intact liver tissue was transferred to ice cold HANKS buffer (ThermoFisher, 14175-079) in a 10cm culture plate. Isolated livers were minced (~2–3mm pieces) with a sterile razor blade, washed twice in hanks buffer by 1 minute settling, and further dissociated for 30 minutes rotating in a 10cm plate at 70RPM (37°C, 5% CO₂, 95% Air) in 24ml liver dissociation solution comprising (66% v/v HANKS buffer, 33% v/v RPMI1640, BSA (0.17% w/v, Sigma-Aldrich), collagenase type 1 (0.3125% w/v, Sigma-Aldrich) and DNase (1U/ml). Following light trituration with a 10ml serological pipette, the homogenate was further dissociated for 10 minutes. The total liver homogenate was filtered (100 μm) and centrifuged at 50xg for 5 minutes to pellet hepatocytes and cell clumps. The supernatant (non-parenchymal fraction, NPC) was pelleted (350xg, 5 minutes) and resuspended in ammonium chloride (STEMCELL Technologies, 07850) for 10 minutes on ice to lyse RBCs. The RBC-free NPC fraction was washed three times (90% HANKS buffer, 10% RPMI1640, 0.05% BSA), filtered (40 μm) and used for surface marker staining as above. The average NPC yield per liver was $10\text{--}25 \times 10^6$ depending on age and sex of the mouse.

Assessment of circulating human specific FVIII levels in NSG mouse plasma was performed on heparinized cardiac or saphenous vein plasma samples following manufacture recommendations (Affinity Biologicals, FVIII-AG, Lot: AG8-0050). Mouse samples were 1:1 – 1:3 diluted to reduce matrix effects and interpolated from a standard curve of human plasma dilutions calibrated to the WHO FVIII antigen standard.

For assessment of *E. coli* bioparticle binding, FACS purified cells ($2\text{--}10 \times 10^4$ cells) were incubated in suspension with AF594-labeled bioparticles (200 particles/cell, ThermoScientific, E23370) in 1ml RPMI1640 with 0.5% BSA supplemented with human IgG (FcR blocking reagent, Miltenyi) for 60 minutes at 37°C. The cells were then washed three times in RPMI1640 with 0.5% BSA to remove unbound particles. Viable human cells free from aggregated bioparticles were assessed for bioparticle binding to CD31⁺ endothelial cells relative to no particle control sorted populations by flow cytometry. For AcLDL-AF488 (Invitrogen, L-23380), and FSA-fitc (D'Liver) ligand binding, purified cells ($5\text{--}10 \times 10^4$ cells) were incubated in suspension with AcLDL-AF488 (2 $\mu\text{g}/\text{ml}$) or FSA-fitc (2 $\mu\text{g}/\text{ml}$) in 300 μl of prewarmed RPMI1640 with 0.5% BSA for 10 minutes at 37°C followed by three washes in RPMI1640 with 0.5% BSA to remove unbound ligands. To assess their ligand uptake ability *in vitro*, dissociated cells were treated with AcLDL-AF488 (2 $\mu\text{g}/\text{ml}$) or FSA-FITC (2 $\mu\text{g}/\text{ml}$) for 10 minutes at 37°C followed by washing and staining with anti-CD31 to quantify endothelial specific uptake of ligands compared to untreated controls by flow cytometry of CD31 and labeled ligands.

Scanning Electron Microscopy of Fenestrations

As a positive control for fenestration structure, freshly isolated non-digested primary human caudate liver tissue was immersed in 2.5% glutaraldehyde and immediate cut into 1–2mm cubes in fixative. After 48 hours of fixation, further processing was performed as below with tissue cubes mounted for *in situ* imaging of the cut sinusoidal and liver tissue surface by SEM. To assess fenestration capacity of *in vitro* hPSC venous-derived LSEC-LCs, HUVECs, and *in vivo* matured day 8 venous angioblast derived LSECs, cells were isolated by FACS or dissociated from adherent culture and seeded on 12mm circular cover glasses (VWR) pre-coated with Matrigel (25% v/v, BD). The cells were seeded as a high-density cell droplet (35–40 μl) in the middle of the coverslip in EGM-2 media (Lonza). After 60 minutes (37°C, 5% CO₂, 95% Air), coverslips were flooded with EGM-2 media for hypoxic culture overnight. Sixteen to eighteen hours later the cells adhering to the coverslip were washed twice with PBS (+Mg/Ca) and fixed in glutaraldehyde (Sigma-Aldrich, 2.5% w/v in PBS, 1–30 days at 4°C). Subsequently coverslips were rinsed in 0.1M Sorenson's phosphate buffer (SPB, pH 7.4)

and placed in 1% OsO₄ (Electron Microscopy Sciences) for 1 hour. Tissue or cells were then rinsed in SPB and dehydrated through an ascending ethanol series then an ascending series of hexamethyldisilazane (HMDS) from 100% ethanol to 100% HMDS. Samples dried overnight in HMDS were mounted on SEM stubs with carbon tape, sputter coated with gold-palladium with a BAL-TEC SCD 050 Sputter Coater and examined with a Hitachi SU3500 Scanning Electron Microscope. Cells were imaged and manually scored for the presence of fenestrations. For these analyses we evaluated ≥ 10 circular transcellular holes between 30-300nm wide arranged in sieve plate clusters. Cells were also analyzed for the general morphology of endothelial cells (smooth cells with regularly spaced angiogenic filopodia) or non-endothelial fibroblast-like cells and rounded cells. Images of *in situ* primary human LSECs and hPSC-derived LSECs (RFP⁺ CD31⁺ CD32⁺, LYVE1⁺) were manually quantified for individual fenestration size by measurement of longest diameter and cell surface area covered by fenestration sieve plates using ImageJ software (Fiji). Histograms of binned fenestration size (20nm bins) were generated using Prism software (Graphpad).

Immunohistochemistry and Immunofluorescence

At various time points after neonatal or adult transplantation (day 15-125), samples of engrafted liver tissue were taken before collagenase perfusion for histological assessment. Samples were fixed in PFA (4%w/v, 24 hours, 4°C, Electron Microscopy Services), then stored in ethanol (70%v/v, 1-30 days, Commercial Alcohols) before paraffin embedding, cutting and immunohistochemical staining by the UHN Pathology Research Program. Sections were imaged at the Advanced Optical Microscopy Facility using a ScanScope AT2 (Aperio) slide scanner with a 40x objective lens and associated ImageScope software (Aperio). Immunohistochemical staining conditions are as follows. Four micron thick FFPE sections were hydrated through decreasing xylene/ethanol/water grades and treated with 3% hydrogen peroxide for 15 minutes. Following antigen retrieval (Tris-EDTA pH9.0) and blocking with serum or 0.5% casein, primary antibodies were applied overnight at 4°C or for 1 hour at room temperature. After rinsing, secondary antibody incubation and development, counterstaining with light Mayer's Hematoxylin was performed before dehydration and mounting. Primary antibodies include: rabbit anti Ku80 (Cell Signaling, 2180, clone C48E7, 1/1000 overnight), rabbit anti human LYVE1 (Abcam, Ab36993, polyclonal, 1/1000 for 1 hour), mouse anti human CD31 (DAKO, M0823, clone JC/70A, 1/50 overnight), goat anti human CD32B (NSJ Bioreagents, R34966, polyclonal, 1/1000 for 1 hour), sheep anti human Stabilin 2 (R&D, AF3645, polyclonal, 1/1000 for 1 hour). Secondary kits and developing reagents, MACH4 (Inter Medico, BC-M4U534L), IMPRESS-AP, (Vector, MP5401-15), developers (Inter Medico, BC-WR806H or DAKO, K3468) were used as per kit instructions.

At similar time points as above, 4 μ m FFPE sections were immunostained for confocal microscopy. Following rehydration, antigen retrieval (Tris-EDTA pH9.0), and casein blocking (DAKO), primary antibodies were applied at 4°C overnight. After three washes in PBS(-/-), secondary antibodies with DAPI counterstain were applied at room temperature for 1 to 2 hours followed by washing and mounting (Prolong Diamond Antifade, Invitrogen) for analysis. Primary antibodies included: rabbit anti LYVE1 (Abcam, AB36993, polyclonal, 1/100), goat anti CD32B (NSJ Bioreagents, R34966, polyclonal, 1/100), mouse anti MRC1 (R&D, MAB253341, clone 685645, 2/100), sheep anti Stabilin2 (R&D, AF3645, polyclonal, 1/100), rabbit anti Ku80 (Cell Signaling, 2180, clone C48E7, 1/100), mouse anti FVIII (Abcam, AB41188, clone 27.4, 2/100), rabbit anti GATA4 (Abcam, Ab84593, polyclonal, 1/100), mouse anti CD31 (DAKO, M0823, clone JC/70A, 2/100), rat anti F4/80 (Bio-rad, MCA497GA, clone Cl:A3-1, 5/100), mouse anti CD34 (BD Biosciences, 340441, clone 8G12, 10/100), rabbit anti SMA (Abcam, Ab32575, clone E184, 1/100), mouse anti Vimentin (Sigma-Aldrich, V6630, clone V9, 1/100), rabbit anti Collagen I (Abcam, Ab34710, polyclonal, 1/100), and rabbit anti Collagen III (Abcam, Ab7778, polyclonal, 1/100). Secondary antibodies included donkey anti host - AF488, AF555, or AF647 variants as appropriate.

To assess protein expression of lineage specification and maturation markers from *in vitro* cultures, CD34⁺ day 8 arterial and venous angioblast populations were prepared by cytopspin and day 12 endothelial cells or day 16 LSEC-LCs were cultured on Matrigel coated 12mm circular coverslips. Cytopspin angioblasts (ThermoFisher, 5x10⁵ cells, 800 RPM, 10 mins) and monolayer cultured endothelial cells were fixed in 4%PFA for 1-2 hours and stored in 5%FCS/PBS until use. Fixed cells were permeabilized in PBS containing 0.1%BSA and 0.2% TritonX for 20 minutes. Following blocking (DAKO, 15 minutes), primary antibodies were applied (4°C, overnight), the cells washed (3 times), and then the secondary antibodies applied with DAPI. Following 1 to 2 hours at room temperature, the cells were washed (3 times) and mounted as described above. The following primary antibodies were used in addition to those for fluorescent slide analysis above: rabbit anti NFATC1 (Abcam, Ab25916, polyclonal, 1/100), rabbit anti HEY2 (Proteintech, 10597-1-AP, polyclonal, 1/100), mouse anti COUTFII (R&D, PP-H7147-00, clone H7147, 1/100), and goat anti VE-CAD (SantaCruz, SC-6458, polyclonal, 5/100). Fluorescently stained samples were imaged at the Advanced Optical Microscopy Facility using a Leica SP8 Confocal imaging system (405nm, 488nm, 552nm, and 638nm laser lines) through HC PL APO CS2 40x/0.85NA dry or HC PL APO CS2 63x/1.40NA oil objective lenses. Images were processed for presentation using ImageJ (Fiji) (Schindelin et al., 2012).

Single-Cell RNA-seq Analysis

Single-cell RNA-seq was performed on a total RFP⁺ population isolated (FACS) at 77 days following neonatal transplantation of day 8 venous angioblasts. The liver tissue was dissociated as described above. DAPI⁻ RFP⁺ live cells were purified by FACS, stored on ice and used immediately for scRNA-seq. Quality control statistics from Cell Ranger are described in Table S1. scRNA-seq data associated with bulk DAPI⁻ RFP⁺ hPSC-derived cells are deposited in GEO: GSE131987. Sample processing was performed as outlined by the 10x Genomics Single Cell 3' v2 Reagent user guide and previously described in detail (MacParland et al., 2018). Briefly, sequencing library generation, data filtering to exclude cells with a high mitochondrial ratio (> 4 SD above mean) and low library size (< 1500), and normalization using scran R package with default settings was performed. Cell clustering using Seurat with

standard procedures, and differential expression analysis as previously described (Innes and Bader, 2018; MacParland et al., 2018), identified 5 primary clusters. Differential gene expression lists for each cluster are provided in Table S2. To identify the cell types that were generated from the hPSC-derived angioblasts, we performed Harmony integration (Korsunsky et al., 2019) with the human liver cell map described by MacParland et al. (GEO: GSE115469). Briefly, the raw count matrixes for 10X single cell experiments of both human primary liver cells and the xenograft-derived cells were merged and processed by our standard pipeline into one Seurat Single Cell Experiment object. PCA was first performed with the raw data to be used for integration. The xenograft-derived cells were integrated with human primary liver cells (as 2 groups: xenograft and primary) using the R package “harmony” (version 0.0.0.9000) by the following parameters: theta = 4, plot_convergence = T, nclust = 15, max.iter.cluster = 100. The resulting clusters were determined by Seurat FindClusters with reduction.type = “harmony,” dims.use = PC1:PC30, and resolution = 0.2. The clusters were visualized by plotting tSNE reduction values on a Cartesian graph. Single-cell results can also be explored in a user-friendly and interactive manner using scClustViz (Innes and Bader, 2018) available at <http://shiny.baderlab.org/hPSCCLSECsAndHumanLiver/>.

To assess similarity between xenograft and various primary liver endothelial and fibroblast subpopulations we performed Pearson correlation analysis using liver cell type signatures. From each of the 20 primary liver cell types, the 50 most differentially expressed genes from each cluster were identified (Table S3). This gene list represented the genes whose expression best distinguished the human liver cell types from each other. From this gene list, we focused our analysis on the differentially expressed genes of primary human liver endothelial (clusters 11, 12, 13) and fibroblast/stellate (cluster 20) clusters, from which we generated a merged and deduplicated 145 gene list (Table S3) that was used for correlation analysis. Statistical correlation between primary liver cells and hPSC-derived *in vivo* matured cells was determined by Pearson correlation with R² values indicating positive or negatively correlating hepatic cell identities for each cluster (0-4) indicated in Figure 6D.

QUANTIFICATION AND STATISTICAL ANALYSIS

All data are represented as mean ± standard error of the mean (SEM). Sample sizes (n) are depicted as individual dots on bargraphs or are specified in figure legends and represent biological replicates as either independent cell culture differentiations or individual mice. For fenestration analysis, sample size (n) represents the number of cells assessed from ≥ three independent mice or differentiation experiments with no statistical analysis performed. No statistical method was used to pre-determine the sample sizes and neither randomization nor investigator blinding was performed on samples. Statistical significance was determined in Prism 8 (Graphpad) software using one-way or two-way ANOVA analysis with Bonferroni post hoc test. Results were considered to be significant at p < 0.05 (*/*#/\$), p < 0.01 (**/*+/#/\$\$), p < 0.001 (***/+++/###/\$\$\$) with specific comparisons indicated in the respective figure legends.

Cell Stem Cell, Volume 27

Supplemental Information

**Generation of Functional Liver Sinusoidal
Endothelial Cells from Human Pluripotent
Stem-Cell-Derived Venous Angioblasts**

Blair K. Gage, Jeff C. Liu, Brendan T. Innes, Sonya A. MacParland, Ian D. McGilvray, Gary D. Bader, and Gordon M. Keller

Generation of functional liver sinusoidal endothelial cells from human pluripotent stem cell-derived venous angioblasts

Blair K. Gage, Jeff C. Liu, Brendan T. Innes, Sonya A. MacParland, Ian D. McGilvray, Gary D. Bader, Gordon M. Keller

Correspondence:

Gordon.keller@uhnresearch.ca (GMK), blair.gage@uhnresearch.ca (BKG)

Supplemental Figures and Tables:

Figure S1, related to Figure 1: Quantification and Optimization of Arterio-Venous Specification.

Figure S2, related to Figure 2: Specification of LSEC-LCs from Venous or Arterial Angioblasts.

Figure S3, related to Figure 2: Effect of Hypoxia/HIF1a Signalling on CD32B Expression.

Figure S4, related to Figures 2, 3, 4, S2, S3 and S7: Isolation and RT-qPCR Characterization of Primary Human LSECs.

Figure S5, related to Figure 5: Histological Characterization of Engrafted Non-Endothelial Cells and Portal Vein Associated Endothelial cells.

Figure S6, related to Figure 6 and Tables S1, S2 and S3: Expression Profiles of hPSC Venous Angioblast-Derived Populations.

Figure S7, related to Figure 1, 2, 3, and 7: Generation of LSEC-LCs and LSECs from H1-GFP hESCs.

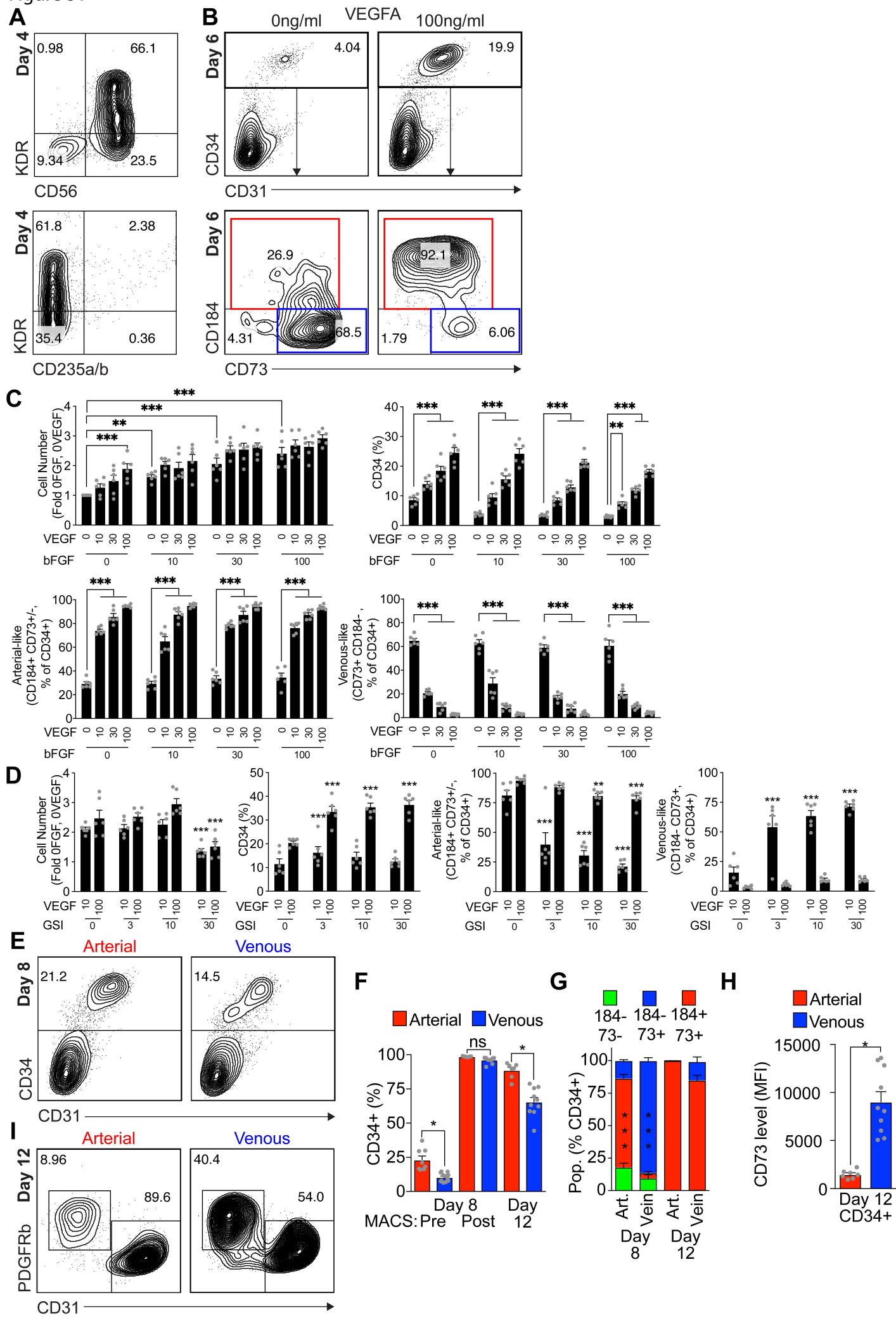
Table S1, related to Figure 6 and S6: scRNA-seq summary statistics.

Table S2, related to Figure 6 and S6: scRNA-seq differentially expressed genes.

Table S3, related to Figure 6: List of differentially expressed genes in the adult liver populations.

Table S4, related to Figures 1, 2, 3, 4, S1, S2, S3, S4, and S7: Primers for Quantitative Reverse Transcription PCR.

Figure S1



Supplemental Figure and Table Legends

Figure S1, related to Figure 1: Quantification and Optimization of Arterio-Venous Specification.

(A) Representative flow cytometric analysis of KDR, and CD56 (upper) and KDR, and CD235a/b (lower) expression on day 4 mesodermal cells. (B) Representative flow cytometric analysis of day 6 CD34⁺ angioblasts specified under different day 4-6 treatment conditions of VEGFA (10, or 100ng/ml), bFGF (30ng/ml). (C-D) Quantification of flow cytometric analysis of day 6 CD34⁺ angioblasts specified with the indicated day 4-6 treatments consisting of VEGFA (0, 10, 30, 100ng/ml), bFGF (0, 10, 30, 100ng/ml) and GSI (0, 3, 10, 30 μ M). (C) Quantification of total cell number (fold normalized to 0ng/ml VEGFA, 0ng/ml bFGF), total CD34⁺ frequency, arterial-like cell frequency (CD34⁺ CD184⁺ CD73^{+/-}, % CD34⁺), and venous-like cell frequency (CD34⁺ CD184⁻ CD73⁺, % CD34⁺) of the populations exemplified in B. ANOVA with Bonferroni test, *p<0.05, **p<0.01, ***p<0.001 between indicated groups. (D) Quantification of total cell number (fold normalized to 0ng/ml VEGFA, 0ng/ml bFGF, 0 μ M GSI in C), total CD34⁺ frequency, arterial-like cell frequency (CD34⁺ CD184⁺ CD73^{+/-}, % CD34⁺), and venous-like cell frequency (CD34⁺ CD184⁻ CD73⁺, % CD34⁺) of populations treated with 30ng/ml bFGF and either 10 or 100ng/ml VEGFA and increasing GSI doses. ANOVA with Bonferroni test, *p<0.05, **p<0.01, ***p<0.001 between indicated groups and 0 μ M GSI control group. (E) Representative flow cytometric analysis of day 8 arterial (day 4-8: 100ng/ml VEGFA and 30ng/ml bFGF) and venous (day 4-8: 10ng/ml VEGFA, 30ng/ml bFGF, and 10 μ M GSI) angioblasts prior to MACS purification. (F-G) Quantification of the frequency of CD34⁺ cells, of arterial and venous angioblasts (day 8) and of derivative CD34⁺ endothelial cells (day 12) following gating strategy indicated in figure 1 C-F. ANOVA with Bonferroni test, *p<0.05, **p<0.01, ***p<0.001 between CD34⁺ populations as indicated and between the day 8 CD34⁺ subpopulations. (H) Mean fluorescence intensity (MFI) of CD73 expression in CD34⁺ day 12 endothelial cells ANOVA with Bonferroni test, *p<0.05 as indicated. Data are represented as mean \pm SEM. (I) Representative flow cytometric analysis of CD31 and PDGFR β expression on total day 12 endothelial populations.

Figure S2

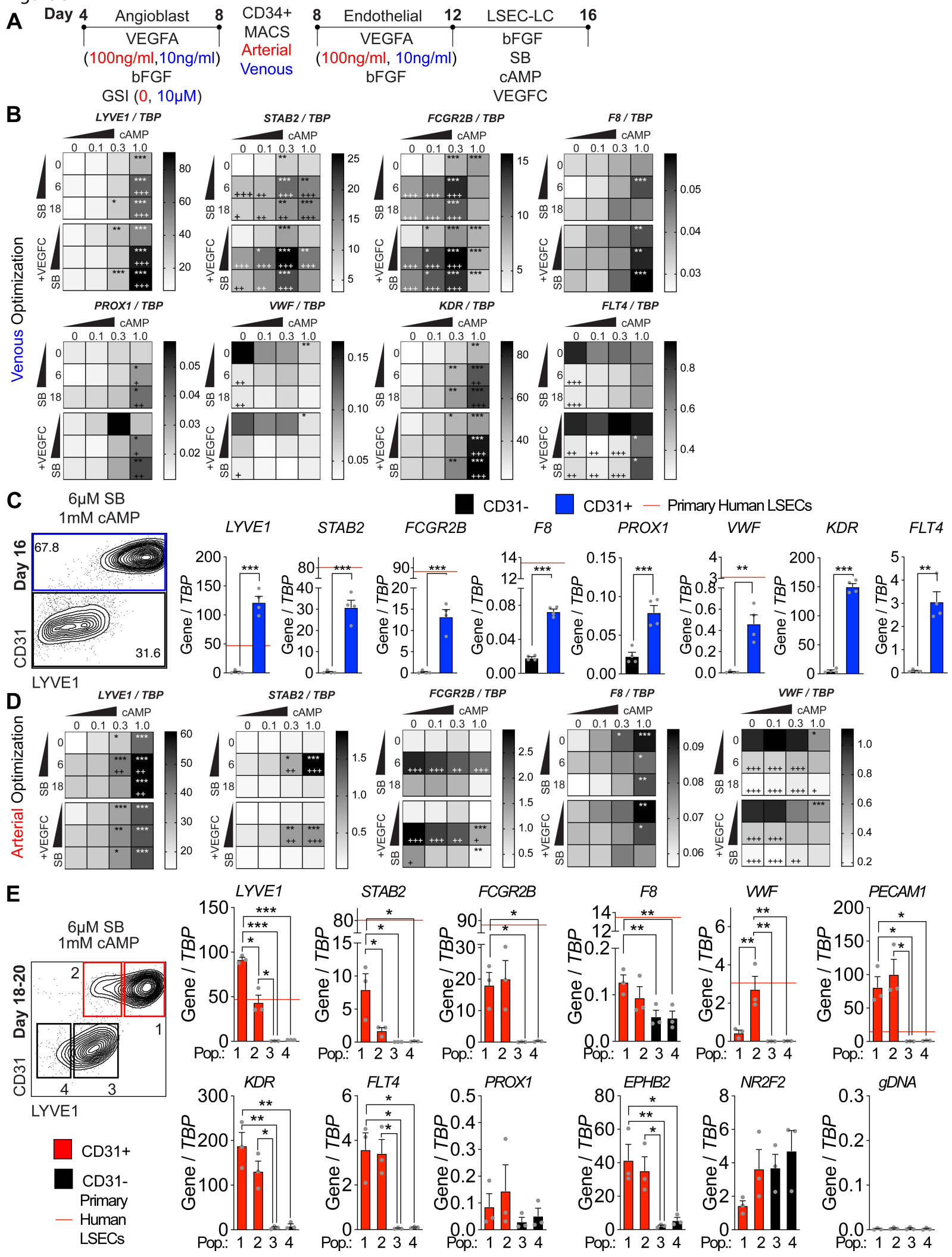


Figure S2, related to Figure 2: Specification of LSEC-LCs from Venous or Arterial Angioblasts.

(A) Schematic of day 4 mesoderm differentiation to arterial or venous angioblasts, endothelial cells and LSEC-like cells (LSEC-LCs). (B) Heatmaps comparing gene expression of LSEC markers and related genes in day 16 venous endothelial cultures after 4 days of treatment with different concentrations of 8-Br-cAMP (cAMP; 0, 0.1, 0.3, 1.0mM), SB-431542 (SB; 0, 6, 18 μ M), and VEGFC (0, 100ng/ml). Each heatmap scale is relative to the indicated gene. ANOVA with Bonferroni test, * $p < 0.05$, ** $p < 0.01$, *** $p < 0.001$ indicated condition vs 0mM cAMP at given SB/VEGFC dose, + $p < 0.05$, ++ $p < 0.01$, +++ $p < 0.001$ indicated condition vs 0 μ M SB / 0ng/ml VEGFC at given cAMP dose. (C) Flow cytometric analyses plot of a day 16 venous endothelial-derived populations indicating the fractions isolated by FACS-mediated purification. RT-qPCR expression analysis of LSEC and general endothelial genes in the isolated CD31⁺ and CD31⁻ populations. ANOVA with Bonferroni test, * $p < 0.05$, ** $p < 0.01$, *** $p < 0.001$ as indicated. (D) Heatmaps comparing gene expression of LSEC markers and related genes in day 18-20 arterial endothelial cultures after 6-8 days of treatment with different concentrations of 8-Br-cAMP (cAMP; 0, 0.1, 0.3, 1.0mM), SB-431542 (SB; 0, 6, 18 μ M), and VEGFC (0, 100ng/ml). Each heatmap scale is relative to the indicated gene (ANOVA with Bonferroni test, * $p < 0.05$, ** $p < 0.01$, *** $p < 0.001$ indicated condition vs 0mM cAMP at given SB/VEGFC dose, + $p < 0.05$, ++ $p < 0.01$, +++ $p < 0.001$ indicated condition vs 0 μ M SB / 0ng/ml VEGFC at given cAMP dose). (E) Flow cytometric analyses plot of a day 18-20 arterial endothelial-derived LSEC-LC population showing the 4 CD31/LYVE1 fractions (Pop.) isolated by FACS mediated purification RT-qPCR analysis of the isolated fractions. ANOVA with Bonferroni test, * $p < 0.05$, ** $p < 0.01$, *** $p < 0.001$, comparing indicated population to populations. For all RT-qPCR analysis, expression values are normalized to levels of the housekeeping gene *TBP*. Where indicated, red line represents the mean expression level of the gene in sorted primary human LSECs. Data are represented as mean \pm SEM.

Figure S3

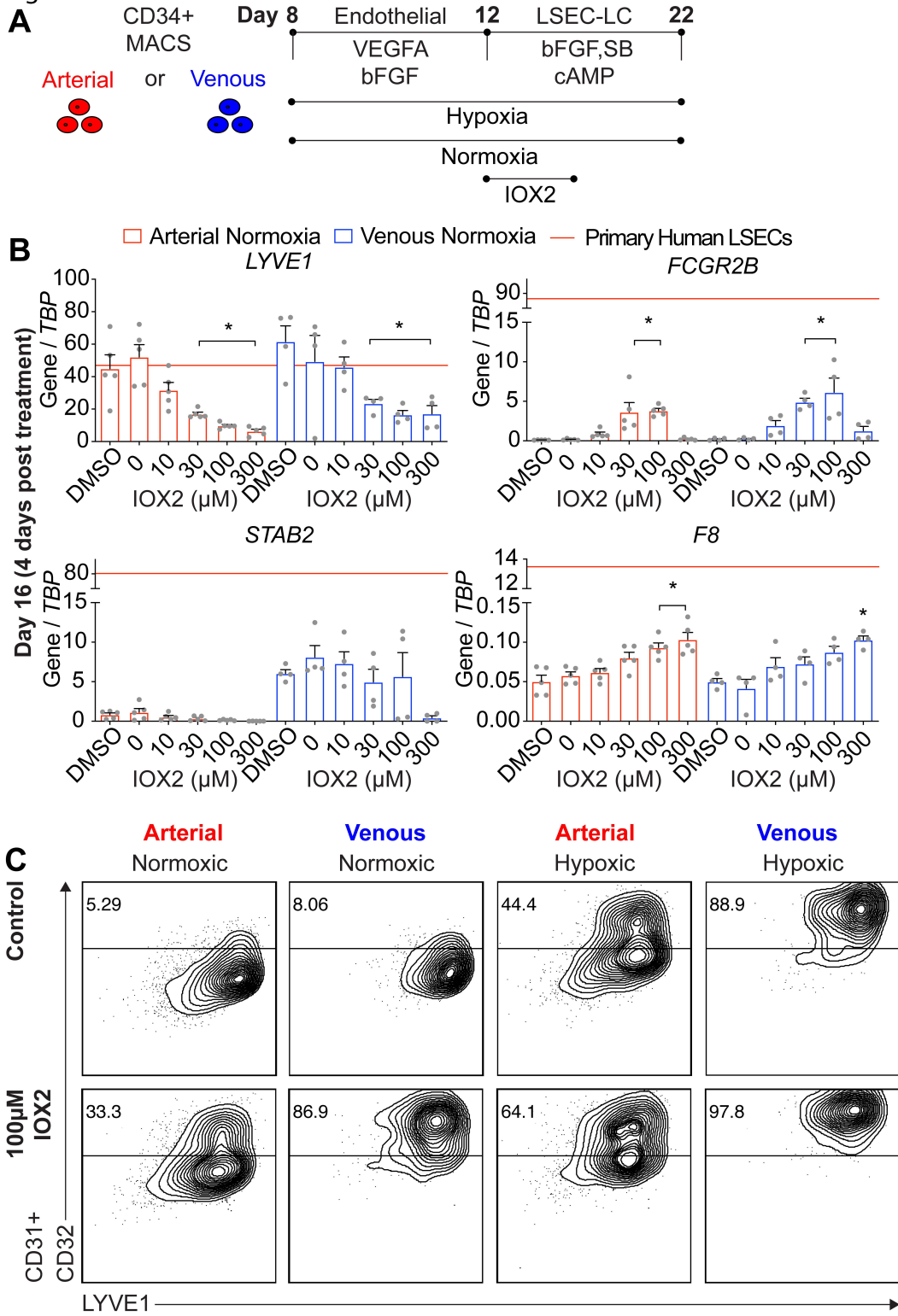


Figure S3, related to Figure 2: Effect of Hypoxia/HIF1a Signalling on CD32B Expression.

(A) Schematic of protocol used to test the effects of IOX2 on the development of arterial and venous LSEC-LCs. IOX2 was added on days 12 and 16 as indicated. (B) RT-qPCR analysis of expression of LSEC markers in day 16 arterial and venous LSEC-LCs cultured under normoxia conditions treated with DMSO or the indicated IOX2 doses for 4 days. ANOVA with Bonferroni test, $*p < 0.05$, comparing arterial and venous cells at given IOX2 doses. (C) Representative flow cytometric analysis of day 16 arterial and venous CD31⁺ LSEC-LCs cultured under normoxic and hypoxic conditions with and without IOX2. For all RT-qPCR analysis, expression values are normalized to levels of the housekeeping gene *TBP*. Where indicated, red line represents mean expression level of the gene in sorted primary human LSECs. Data are represented as mean \pm SEM.

Figure S4

A Primary Human LSEC Sort from Non-Parenchymal Cells

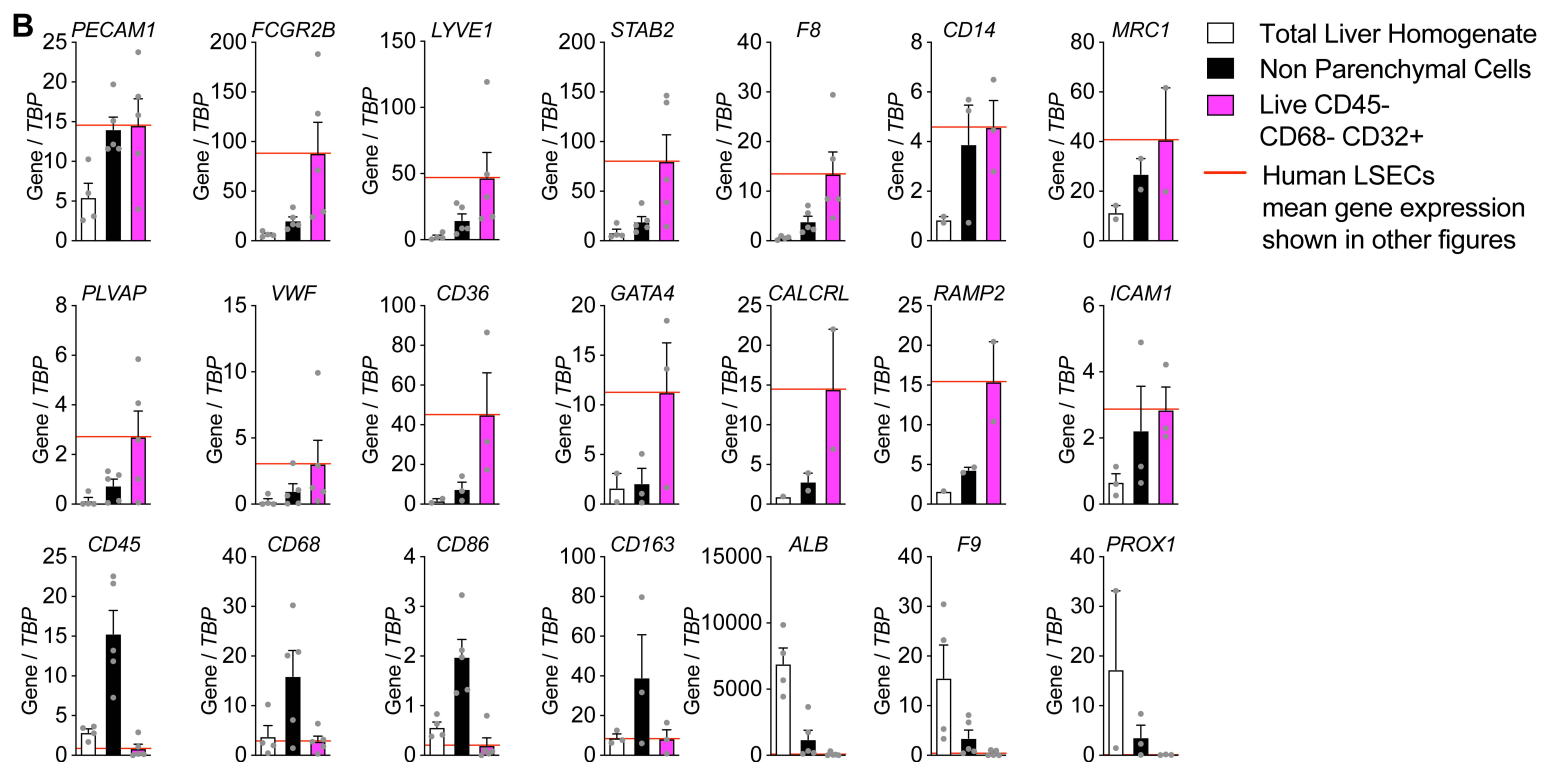
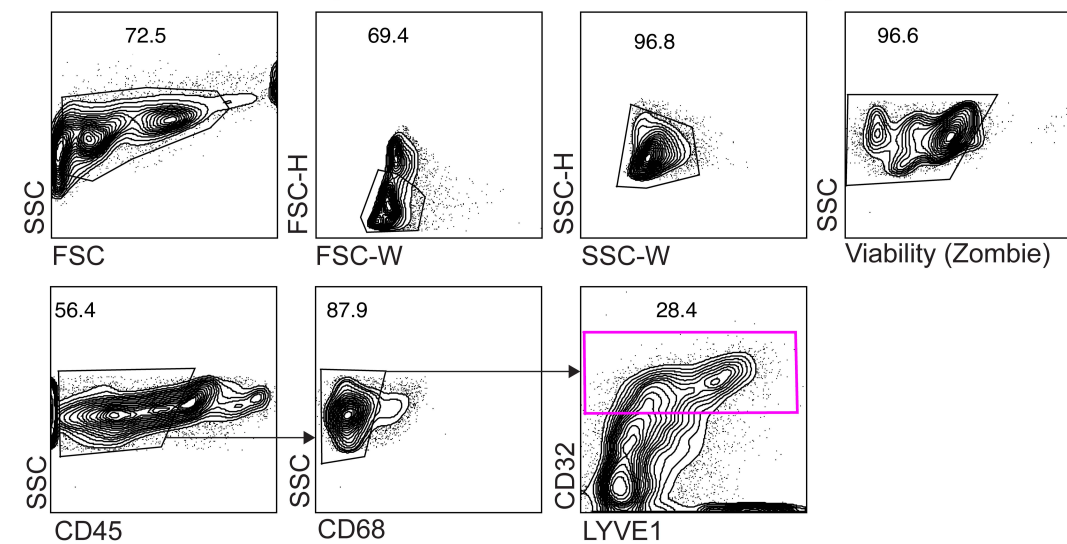


Figure S4, related to Figures 2, 3, 4, S2, S3 and S7: Isolation and RT-qPCR Characterization of Primary Human LSECs.

(A) FACS strategy used to isolate primary human LSECs from the non-parenchymal cell (NPC) fraction of enzymatically dissociated human caudate lobe tissue. Live, single-cell populations, depleted of CD45⁺ /CD68⁺ hematopoietic cells and macrophages were isolated based on CD32 expression. This population includes cells that express intermediate to high levels of LYVE1. (B) RT-qPCR based expression of the indicated in genes in the total liver homogenate, the hepatocyte-depleted non-parenchymal cell fraction, and the CD45⁻CD68⁻CD32⁺ primary human LSEC populations. Red line indicates mean expression value that is depicted in other figures in the manuscript. For all RT-qPCR analyses, expression values are normalized to levels of the housekeeping gene *TBP*. Data are represented as mean \pm SEM.

Figure S5

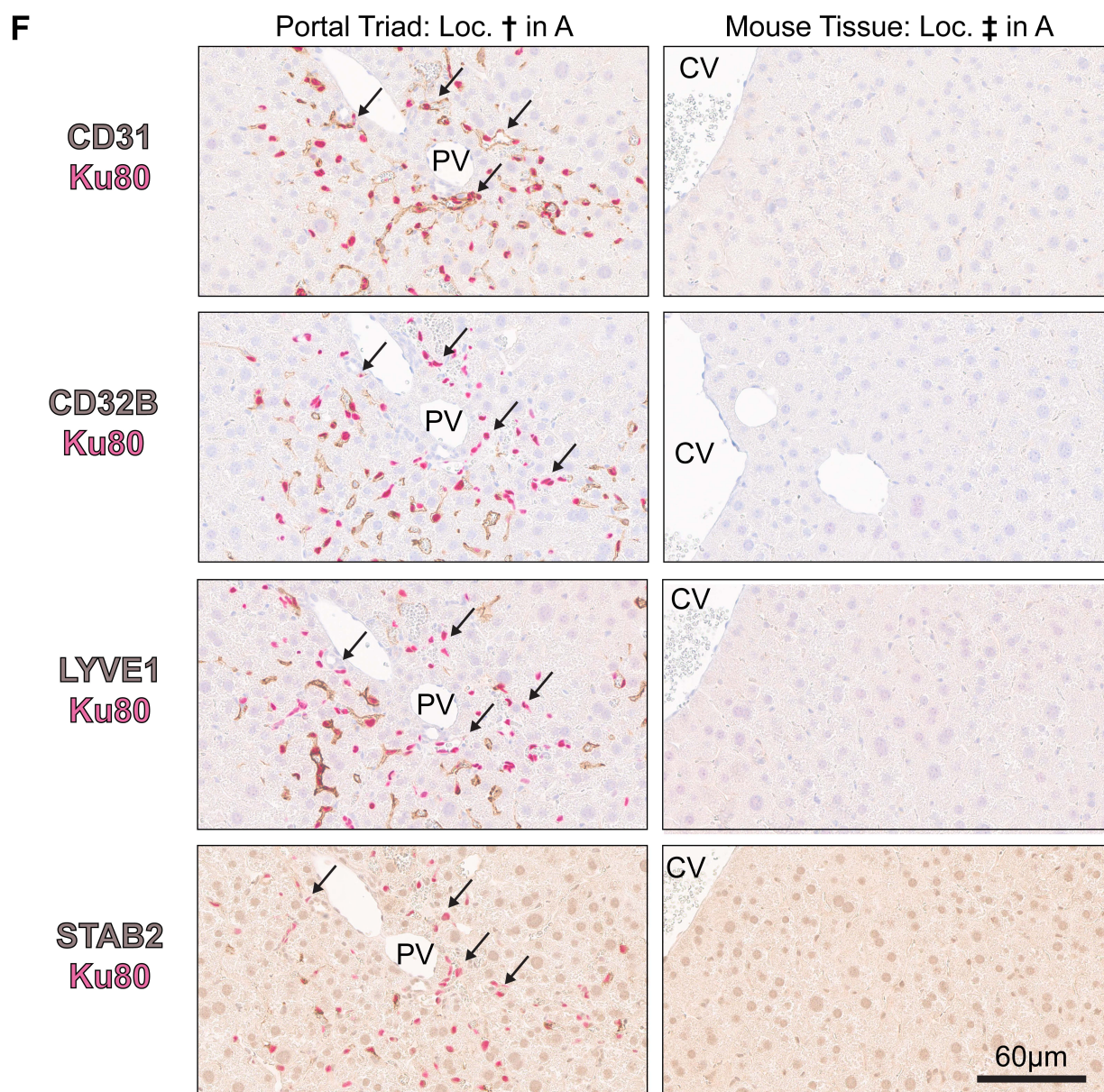
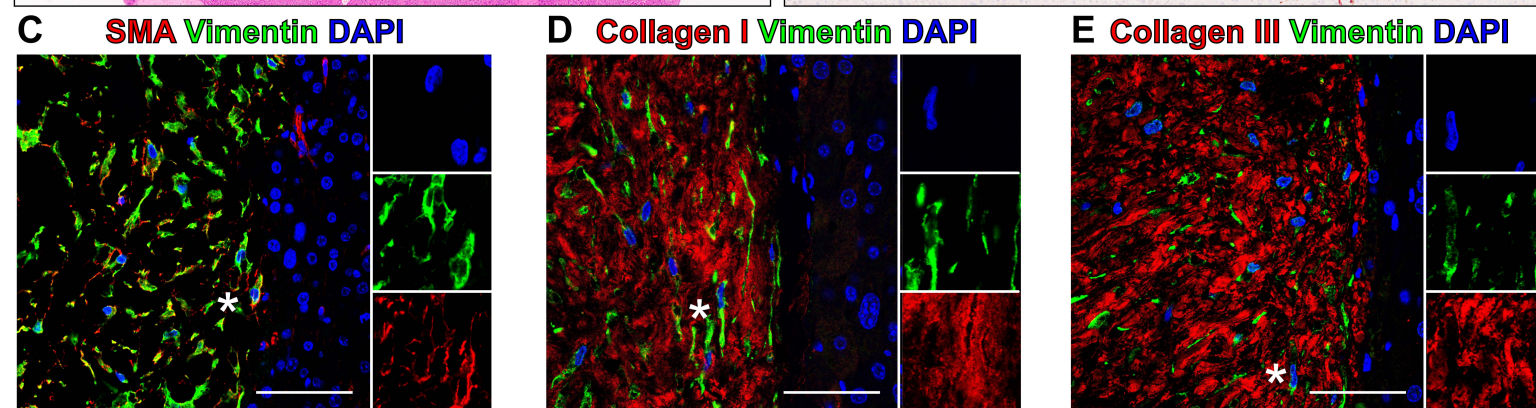
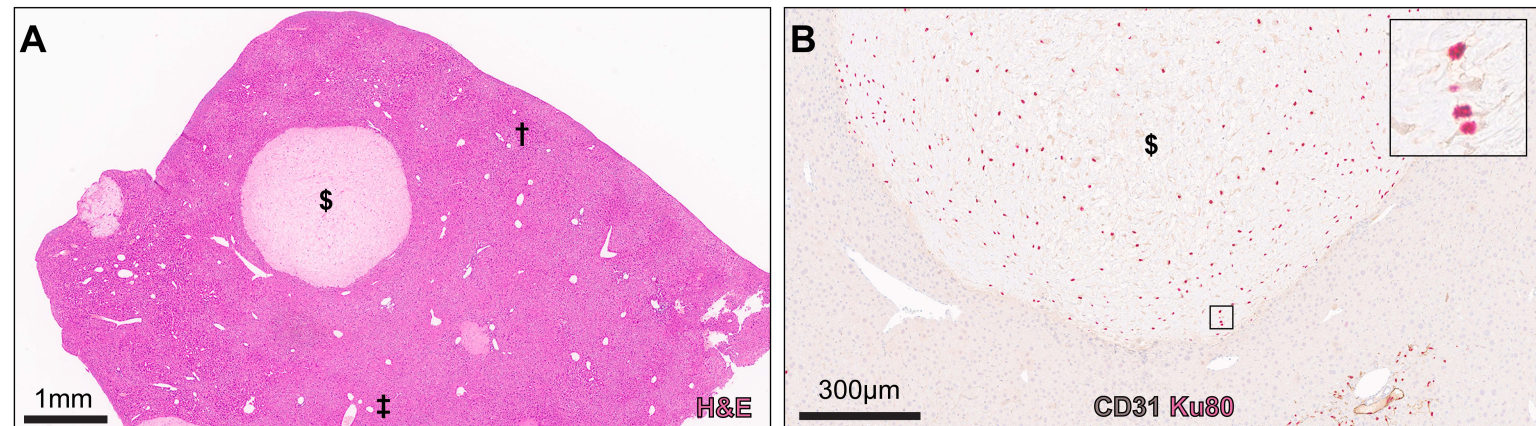


Figure S5, related to Figure 5: Histological Characterization of Engrafted Non-Endothelial Cells and Portal Vein Associated Endothelial cells.

(A-B) Histological analysis of the endothelial engrafted regions of a NSG mouse liver 88 days following neonatal transplantation of day 8 venous angioblasts. (A) Low magnification Hematoxylin and Eosin stained section depicting regions where serial sections are located in other panels including, a zone 1 peri-portal engrafted region, (single dagger, †, shown in F), a non-engrafted region (double dagger, ‡, shown in F) a non-endothelial nodule (dollar sign, \$, shown in B). (B) Histological analysis of a nodule staining negative for human specific CD31 (brown) and positive for Ku80 (human cells, pink). Black box indicates area of enlarged inset. (C-E) Immunofluorescence staining of fibroblast associated markers (SMA, vimentin, collagen I, and collagen III) within the non-endothelial human-derived nodule. Left side of each image is within the nodule border with surrounding liver tissue on the right. "*" indicates location of enlarged single channel inset panels with colours as indicated. Scale bars are 50µm. (F) Left Panel: histological analyses of portal triad associated engraftment showing human endothelial cells that express CD31 but not LYVE1, CD32B, or STAB2 (black arrow heads). Right panel: identically stained non-engrafted mouse liver tissue depicting human specificity of histological assessment. Scale bars are 60µm.

Figure S6

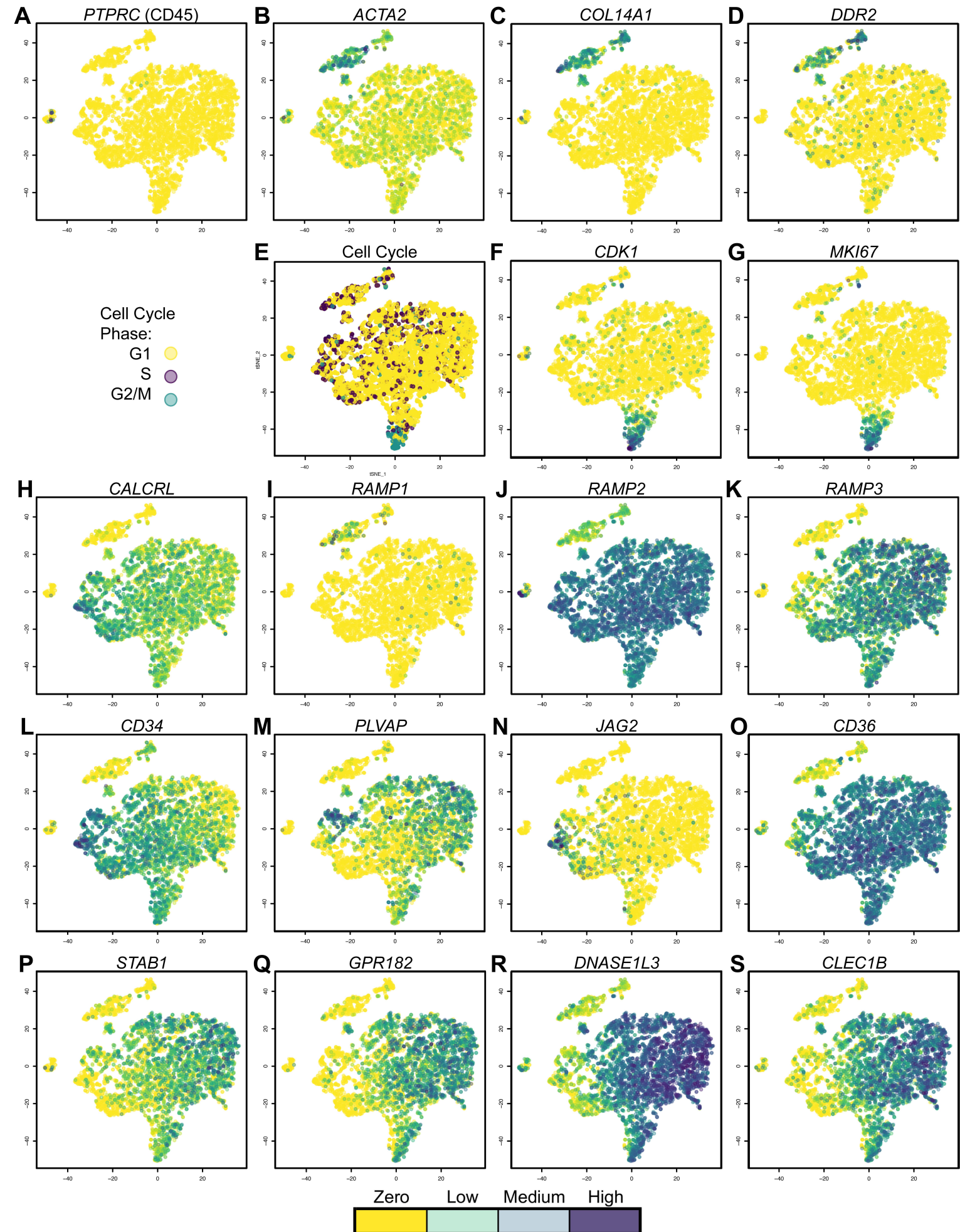


Figure S6, related to Figure 6 and Tables S1, S2 and S3: Expression Profiles of hPSC Venous Angioblast-Derived Populations.

Expression patterns of genes associated with the LSEC lineage. (A) Expression of *PTPRC* (CD45) is included as a marker of hematopoietic cells. (B-D) Expression of candidate fibroblast/smooth muscle/mesenchymal markers, (E) Expression of predictive cell cycle status of all cells, (F-G) Expression of candidate cell cycle progression associated markers, (H-K) Expression of receptors and co-receptors of adrenomedullin signalling pathway, (L-S) Expression of LSEC and endothelial markers.

Figure S7

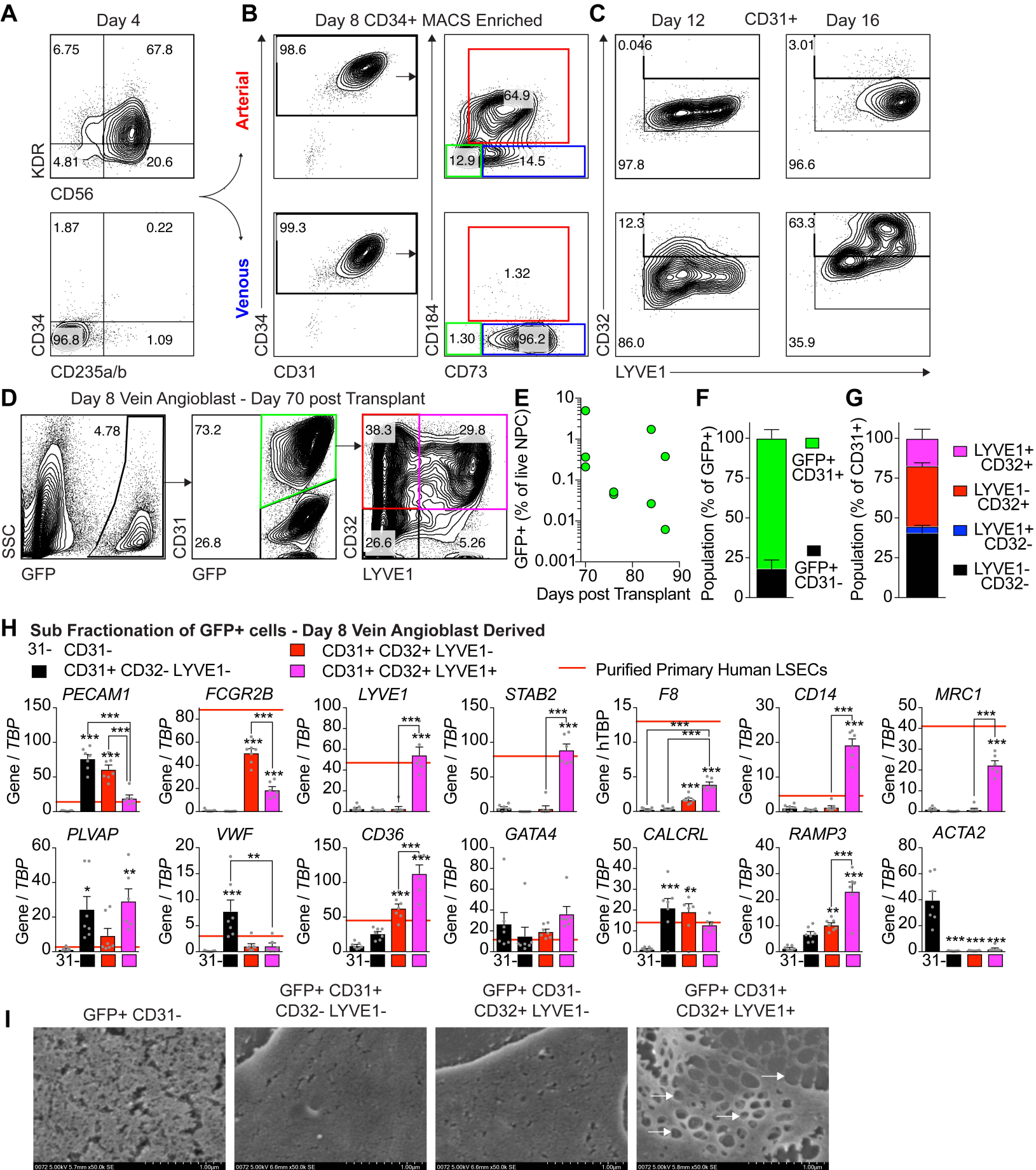


Figure S7, related to Figure 1, 2, 3, and 7: Generation of LSEC-LCs and LSECs from H1-GFP hESCs.

(A) Representative flow cytometric analysis of KDR, CD56, CD34 and CD235a/b expression on H1-derived day 4 mesodermal cells induced with the protocol shown figure 1A. (B) Representative flow cytometric analysis of CD34, CD31, CD184 and CD73 expression on CD34⁺ MACS isolated day 8 arterial and venous angioblasts specified (day 4-8) with 100ng/ml VEGFA (arterial) and 10ng/ml VEGFA and 10 μ M GSI (venous) respectively. (C) Representative flow cytometric analysis of CD32 and LYVE1 expression on CD31⁺ arterial and venous LSEC-LCs induced under hypoxic conditions as indicated in figure 2A. (D) Representative flow cytometric analysis of the NPC fraction of the livers of mice transplanted (neonatal) for 70-days with H1-derived day 8 venous angioblasts. (E) Proportion of GFP⁺ cells in the NPC fraction of the livers of the engrafted mice transplanted for 70-87 days. (F) Proportion of CD31⁺ cells in the GFP⁺ hPSC-derived population. (G) Proportion of CD32 and LYVE1 expressing cells in the GFP⁺CD31⁺ population. (H) RT-qPCR expression analyses of indicated LSEC genes in the CD31⁻, CD31⁺CD32⁻LYVE1⁻, CD31⁺CD32⁺LYVE1⁻, CD31⁺CD32⁺LYVE1⁺ populations isolated from livers engrafted with day angioblasts for 70-87 days. (ANOVA with Bonferroni test, *p<0.05, between GFP⁺ CD31⁻ cells and indicated samples or additionally as indicated between GFP⁺ CD31⁺ fractions). For all RT-qPCR analysis, expression values are normalized to levels of the housekeeping gene *TBP*. Where indicated, red line represents the mean expression level of the gene in sorted primary human LSECs. Data are represented as mean \pm SEM. (I) Scanning electron microscopic-based analyses of fenestrations in the indicated populations isolated from livers engrafted for 84 days with day 8 venous angioblasts. Imaging conditions and scale bar are indicated below each image.

Table S1

Estimated Number of Cells

5,280

Mean Reads per Cell

40,751

Median Genes per Cell

2,075

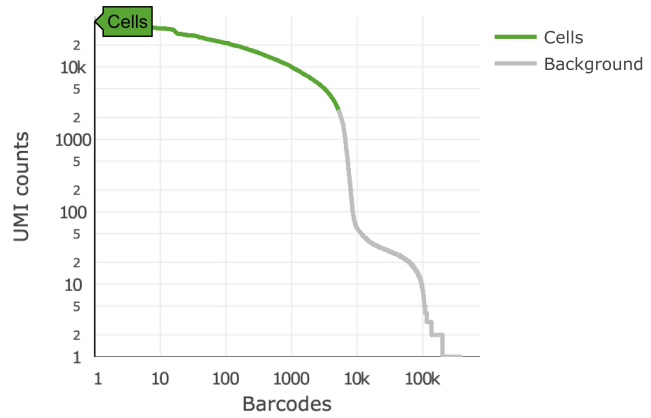
Sequencing

Number of Reads	215,168,467
Valid Barcodes	98.1%
Sequencing Saturation	60.9%
Q30 Bases in Barcode	96.8%
Q30 Bases in RNA Read	73.8%
Q30 Bases in Sample Index	88.0%
Q30 Bases in UMI	95.6%

Mapping

Reads Mapped to Genome	84.0%
Reads Mapped Confidently to Genome	81.4%
Reads Mapped Confidently to Intergenic Regions	3.0%
Reads Mapped Confidently to Intronic Regions	23.6%
Reads Mapped Confidently to Exonic Regions	54.9%
Reads Mapped Confidently to Transcriptome	52.0%
Reads Mapped Antisense to Gene	1.0%

Cells



Estimated Number of Cells	5,280
Fraction Reads in Cells	87.8%
Mean Reads per Cell	40,751
Median Genes per Cell	2,075
Total Genes Detected	21,064
Median UMI Counts per Cell	5,742

Sample

Name	Keller_Blair__BGTX7_d77ptx_M2T8V_RFP
Description	
Transcriptome	GRCh38
Chemistry	Single Cell 3' v2
Cell Ranger Version	2.1.0

Table S1, related to Figure 6 and S6: scRNA-seq summary statistics.

Sample summary statistics associated with the 77-day post-transplant hPSC-derived venous angioblast origin DAPI⁻ tdRFP⁺ population. Statistics are those generated by default data processing by 10X Genomics Cell Ranger software version 2.1.0.

Table S2, related to Figure 6 and S6: scRNA-seq differentially expressed genes.

Differentially expressed gene lists for each of the five clusters (Cluster 0, 1, 2, 3, 4).

Table S3, related to Figure 6: List of differentially expressed genes in the adult liver populations.

List of the top 50 differentially expressed genes between each of the 20 clusters (clusters 1-20; "S1-S20") in primary human liver as reported by MacParland et al. (2018). Gene expression levels for the 1000 genes are depicted including expression levels in hPSC-derived clusters (clusters 0-4). Pearson correlation analysis (Figure 6E) used the 200 human liver and endothelial subtyping genes (50 genes from 4 clusters) after removal of low expression and duplicate genes between the groups (145 genes).

Table S4, related to Figures 1, 2, 3, 4, S1, S2, S3, S4, and S7: Primers for Quantitative Reverse Transcription PCR.

List of single exon targeting primers used for RT-qPCR analysis in this study. Note that "gDNA" primers target the untranscribed upstream promoter element of *PAGE1* (*GAGEB1*) serving to detect gDNA contamination in reverse transcribed cDNA samples.